journal of the international meteor organization

WGN

47:5
october 2019

Meteor shower activity profiles using the D criteria
Legendary showers studied on Harvard photographic results
Fast video thresholding options to obtain pixel exceedances
December Rho Virginids and Comet C/1961 T1 (Seki)
September IMO video meteors

ISSN 1016-3115

WGN Vol. 47, No. 5, October 2019, pp. 133 – 164

Administrative

Meteor science

Preliminary results

Front cover photo

Bright fireball above the observatories at Provence-Alpes-Côte d'Azur, France at $21^{\mathrm{h}}02^{\mathrm{m}}$ UT on 2019 September 23. Photo courtesy: Mikael De Ketelaere.

Writing for WGN

This Journal welcomes papers submitted for publication. All papers are reviewed for scientific content, and edited for English and style. Instructions for authors can be found in WGN **45:1**, 1–5, and at `http://www.imo.net/docs/writingforwgn.pdf` .

Copyright

Legal address

International Meteor Organization, Jozef Mattheessensstraat 60, 2540 Hove, Belgium.

From the Treasurer — IMO Membership/WGN Subscription Renewal for 2020

Marc Gyssens

Renewal rates

Most members/subscribers whose membership/subscription has expired should have received a reminder email. Via this way, we invite them again to renew for 2020.

The fees are as tabulated below. We are happy that we can offer WGN at the same cost as last year. We also continue to offer an electronic-only subscription at a reduced rate.

IMO Membership/WGN Subscription 2020				
Electronic + paper with surface mail delivery:		€26		US$ 32
Electronic + paper with airmail delivery (outside Europe only):		€49		US$ 60
Electronic only:		€21		US$ 25
Supporting membership:	add	€26	add	US$ 32

It is also possible to renew for two or more years in a row.

When you renew, give a few minutes of thought to becoming a **supporting member** by paying at least 26 EUR/32 USD extra. Smaller gifts are of course also appreciated. As you may know, there is an IMO Support Fund. With this Support Fund, we offer support to meteor-related projects. Our ability to provide this service to the meteor community depends primarily on the gifts we receive from supporting members!

Another way to help meteor workers with limited funds is to offer them a gift subscription.

We already thank all our members that will renew for their continued trust in our Organization!

Payment instructions

If you are not yet familiar with the new IMO website, you first must log in into your account if you want to renew. For this purpose, click the log-in button in the upper right-hand corner. As login, use the email address on which you received my reminder email. In case you forgot your password, you can use the "forgot password" link to reset it. Once logged in, you will see your profile picture (or the space provided for it). If you read on the green button below it that your membership is about to expire, click it, and the rest will be self-explanatory.[1]

The outcome of this process is that you will see the total amount due and your payment options. If you choose to pay using PayPal (or using a credit card via PayPal), you can complete the payment on our website.

If you experience any difficulties, do not hesitate to contact me at `treasurer@imo.net`.

One final request: every year, a lot of members renew late. As a consequence, back issues that already appeared have to be sent out to these members. Please support our volunteers in their bimonthly effort to have WGN shipped to you by renewing promptly! Thank you for your understanding and cooperation!

[1] Alternatively, you can also click on "Extend your membership" in the pull-down menu to the right of your name in the upper right-hand corner, with the same result.

Meteor science

Meteor shower activity profiles and the use of orbital dissimilarity (D) criteria

Althea V. Moorhead[1]

Orbital dissimilarity, or D, criteria are often used to select members of a meteor shower from a set of meteor observations. These criteria provide a quantitative description of the degree to which two orbits differ; if the degree of dissimilarity between a shower's reference orbit and an individual meteor does not exceed a selected threshold, the meteor is considered to be a member of that shower. However, members of a meteor shower tend to disperse in longitude of the ascending node (and thus in solar longitude) while preserving a common Sun-centered ecliptic radiant. Employing dissimilarity criteria to judge shower membership may therefore make the shower appear briefer than it actually is. We demonstrate this effect for two simulated meteor showers and assess the maximum permitted deviation in solar longitude as a function of radiant and velocity measurement error.

Received 2019 September 4

1 Introduction

Meteor showers are transient but typically annually recurring phenomena in which groups of meteors with similar orbits intersect the Earth. Because they have similar orbits, they tend to intersect the Earth with the same speed, radiant (or directionality), and solar longitude (time of year). The activity level of a shower is often described in terms of zenithal hourly rate, or ZHR, which is the number of visual meteors that would be seen under ideal observing conditions when the radiant is directly overhead. Thus, the basic set of parameters describing a meteor shower typically include a peak solar longitude, radiant, geocentric speed, and peak or maximum ZHR.

The peak or maximum ZHR describes the intensity of a meteor shower only during its most active night (or hour). The shower will also produce off-peak activity, albeit at a lower rate. Unless a shower exhibits multiple peaks, the ZHR increases steadily before and decays after the peak date and time. The "sharpness" of the peak, or the rise and decay time, can vary substantially between showers. For instance, the Quadrantids are a very brief shower, with measurable activity lasting only 2-3 days. In contrast, the Northern and Southern Taurids can last weeks, if not months. In most cases, the rise, peak, and decay in a shower's activity can be characterized as a double-exponential profile (Jenniskens, 1990; Jenniskens, 1994; Olech et al., 1999; Dubietis & Arlt, 2002; Moorhead et al., 2017).

An accurate description of the change in a meteor shower's activity over time has multiple uses. It can be used to plan observations, or to calibrate off-peak flux measurements. It is critical for generating meteor shower forecasts (McBride, 1997; McDonnell et al., 2001; Moorhead et al., 2017; Moorhead et al., 2019); if spacecraft operators are to mitigate the increased risk of damage posed by a meteor shower, they must know how long a shower lasts in addition to when it occurs.

Within a set of meteor data, showers appear as time-limited concentrations in meteor radiant and speed. The time-limited requirement distinguishes meteor showers from sporadic sources; the latter appear as concentrations in Sun-centered ecliptic radiant and, to a lesser extent, speed that persist throughout the year. The sporadic sources exhibit seasonal variations in strength (Campbell-Brown & Jones, 2006) but at no point do they become inactive. If a shower's Sun-centered ecliptic radiant lies near one of these sporadic sources, false positives for shower membership will occur at a higher rate. There may be no way to filter out these false positives individually, but the rate of false positives can be measured as shower "activity" far from the peak (Moorhead, 2016). This false positive rate can be used to measure a detected shower's signal-to-noise ratio (Brown et al., 2008).

In order to study a given meteor shower, we generally must separate the members of that shower from a data set that contains both shower and sporadic meteors. This is generally accomplished by selecting the meteors that are most similar to some set of reference parameters for the shower; these parameters may be either a radiant, speed, and solar longitude, or they may be a set of orbital elements. Often, so-called dissimilarity, or D, parameters are used (Southworth & Hawkins, 1963; Drummond, 1981; Jopek, 1993; Valsecchi et al., 1999). These parameters distill the difference between two orbits into a single number that is larger for more disparate orbits. As a result, similarity in one parameter can compensate for dissimilarity in another. Thus, meteors with more disparate radiants may be included near the time of the peak, when the solar longitude or ascending node is more similar to that of the shower. If measurement error in radiant and velocity is independent of observation time, this may narrow the apparent duration of the shower's activity.

In this paper, we demonstrate this shortening of the shower's activity using simple simulations of meteor

[1]NASA Meteoroid Environment Office, Marshall Space Flight Center, Huntsville, AL 35812, USA
Email: althea.moorhead@nasa.gov

IMO bibcode WGN-475-moorhead-profiles
NASA-ADS bibcode 2019JIMO...47..134M

showers. We construct our artificial meteor showers by assuming that their activity as a function of solar longitude can be described by a double-exponential profile and that both the Sun-centered radiant and geocentric speed of each shower remains constant over time. We also construct "noise" meteors, or potential false positives for shower association, that have the same distribution of Sun-centered radiant and geocentric speed but are equally likely to occur at any solar longitude. We then select shower members using two approaches. First, we apply a simple cut in radiant and geocentric velocity. Second, we apply the Drummond D parameter (Drummond, 1981) in conjunction with the cutoff values recommended by Galligan (2001). These methods are by no means exhaustive, but serve to demonstrate that in some cases, member extraction using D parameters can artificially steepen the apparent activity profile.

2 Methods

This section describes our methods for generating simple simulated meteors, our assumed shower parameters, and the manner in which we have estimated a noise level.

2.1 Generation of simulated meteors

We generate a radiant, speed, and solar longitude for each simulated meteor. First, we generate solar longitudes by assuming that the activity profile of the shower follows a double exponential profile (Jenniskens, 1994; Moorhead et al., 2017):

$$\mathrm{ZHR} \propto \begin{cases} 10^{+B_p(\lambda_\odot - \lambda_0)} & \lambda_\odot < \lambda_0 \\ 10^{-B_m(\lambda_\odot - \lambda_0)} & \lambda_\odot > \lambda_0 \end{cases} \quad (1)$$

Thus, we adopt a form of this equation as the probability distribution for generating random solar longitude values (see Figure 1).

We also assume that noise will be present in the shower at some level. We model this noise as meteors that have the same radiant and velocity distribution as shower members, but are equally likely to occur for any solar longitude. We generate these "noise" meteors by selecting random solar longitudes that lie within 90° of the peak. The noise level varies by shower and is expressed as a percentage; if, say, the assumed noise level is 20% and the total number of simulated meteors is 5000, then 1000 will be noise meteors and 4000 will be shower meteors.

In order to calculate simulated meteor radiants, we assume that the shower radiant remains at the same value of Sun-centered ecliptic longitude and latitude (see, e.g., Brown et al., 2010); the typical drift of a shower radiant in these coordinates is less than one degree (Peter Brown, personal comm.). We then assume that the meteors are observed by a camera system with a relatively low level of precision, and thus that the measured radiants are scattered about the true radiant in a circularly symmetric fashion, with a normal distribution in angular radiant offset. We set the standard deviation of this offset distribution to 3°. The distribution of Sun-centered ecliptic longitude and latitude, and the corresponding values of right ascension and declination, are depicted in Figure 2.

Finally, we assume that the spread in observed meteoroid speeds is also dominated by measurement error. We generate meteoroid speeds using a normal distribution centered on the true shower speed, with a standard deviation of 10% of the shower speed (see Figure 3).

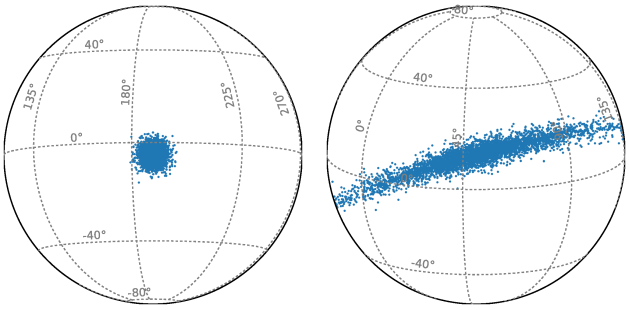

Figure 2 – Simulated Sun-centered ecliptic longitude and latitude (left) and right ascension and declination (right) for the Southern Taurid meteor shower.

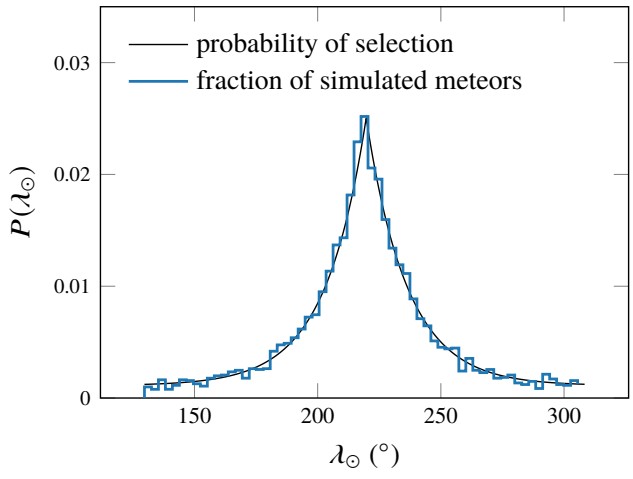

Figure 1 – Solar longitude probability distribution (black line) and normalized histogram of simulated solar longitude values (thick blue line) for the Southern Taurid meteor shower.

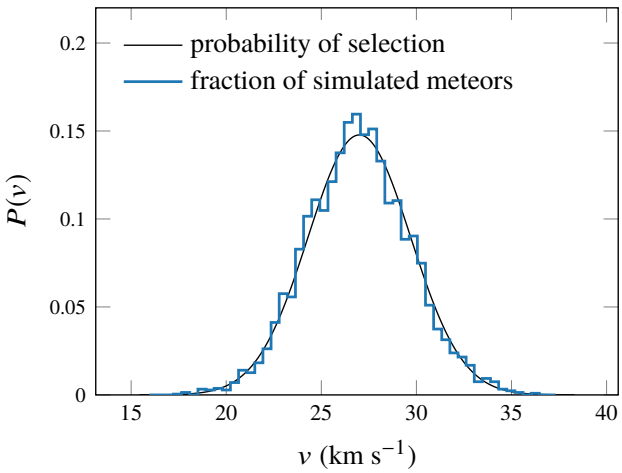

Figure 3 – Velocity probability distribution (black line) and normalized histogram of simulated meteoroid speeds (thick blue line) for the Southern Taurid meteor shower.

Table 1 – Shower parameters used to generate simulated Perseid and Southern Taurid meteors. The solar longitude, right ascension, declination, and orbital elements are those of the shower at its peak or maximum activity.

		Perseids	Southern Taurids
solar longitude	$\lambda_\odot$	140.05°	219.7°
	B	0.35	0.026
right ascension	R.A.	47.2°	50.1°
declination	dec.	57.8°	13.4°
Sun-centered ecliptic longitude	$\lambda_\odot - \lambda_g$	282.44°	188.23°
ecliptic latitude	β_g	38.38°	−4.83°
geocentric speed	v_G	59 km s^{-1}	27 km s^{-1}
perihelion	q	0.96 au	0.38 au
eccentricity	e	0.93	0.81
inclination	i	113.3°	5.3°
argument of pericenter	ω	151.6°	113.1°
longitude of ascending node	Ω	140.0°	39.7°
maximum dissimilarity	$D_{\max}$	0.18	0.06
noise level		1%	20%

These simulated solar longitudes, radiants, and velocities are then converted to orbital elements by combining the meteor's geocentric velocity vector with the Earth's position at the given solar longitude in 2019 to create a complete state vector.

2.2 Assumed shower parameters

We will present results for two test cases: the Perseids and the Southern Taurids. The Perseids are a major meteor shower that lasts approximately a couple weeks; the Taurids are less active at any given time, but have a much longer duration. In fact, using the rise and decay time measured by Jenniskens (1994), Taurid activity lasts 3-6 months. Thus, we expect the use of D-parameters to select members of each shower to affect the Taurid activity profile more strongly than the Perseid activity profile. The full list of parameters used to simulate these showers is given in Table 1. Both the Perseids and the Southern Taurids are typically modeled as having symmetric activity profiles; that is, $B_p = B_m$ (Jenniskens, 1994; Moorhead et al., 2019). We therefore drop the subscripts and provide a single B value for each shower. We also calculate the orbital elements for each shower at the time of the peak using the same approach described in the previous section.

These values are assembled from a variety of sources. The peak solar longitude and B values are taken from either SonotaCo (2009), in the case of the Southern Taurids, or Moorhead et al. (2019), in the case of the Perseids. The right ascension (R.A.), declination (dec.), and approximate geocentric speed (v_g) for both showers are taken from SonotaCo (2009). The cutoff D parameter, which we will refer to as $D_{\max}$, is taken from Galligan (2001). These maximum D values are intended to recover 70% of the stream and vary depending on the inclination of the shower.

2.3 Noise level

The final parameter needed to generate our simulated data is the noise level. We roughly estimate the noise using meteor data from the NASA All-Sky Fireball Network (Cooke & Moser, 2012). For each shower, we select meteors that fall within 5° of each shower's Sun-centered ecliptic radiant and within 20% of the shower's geocentric velocity. We then compare the number of meteors meeting this criteria whose solar longitudes lie more than 90° away from the peak solar longitude to those that lie within 90° of the peak. We take the former to be N_{noise} and the latter to be $N_{\text{signal}} + N_{\text{noise}}$ for the six-month period encompassing the peak.

The Perseids produce a large number of fireballs and thus are strongly represented in our data set; they also have fairly little contamination from the sporadic background. Thus, $N_{\text{noise}}/(N_{\text{signal}} + N_{\text{noise}}) \simeq 1\%$ for the Perseids. In contrast, the Southern Taurids lie near the antihelion source and are strongly contaminated with false positives. We estimate the noise level for the Southern Taurids at about 20%. Note that these noise levels are system dependent; systems with a lower limiting meteoroid mass, for instance, will likely detect proportionately more sporadic meteors and thus have a higher noise level.

3 Shower extraction

3.1 Method 1

We select shower members from our simulated data using one of two methods. In the first method, we select those meteors that lie within 5° of the Sun-centered ecliptic shower radiant and within 20% of the geocentric shower speed. 86% of meteors in both showers satisfy these criteria, regardless of whether they are shower meteors or "noise" meteors.

3.2 Method 2

In the second method, we compute the orbital dissimilarity between the meteors and the shower using the Drummond D-parameter. This parameter is:

$$D^2 = \left(\frac{q_m - q_s}{q_m + q_s}\right)^2 + \left(\frac{e_m - e_s}{e_m + e_s}\right)^2 + \left(\frac{I}{180°}\right)^2 + \left(\frac{e_m + e_s}{2} \cdot \frac{\theta}{180°}\right)^2 \quad (2)$$

where q is perihelion distance, e is orbital eccentricity, and i is orbital inclination. The subscripts indicate whether the parameter is that of the shower (s) or of an individual meteor (m). The terms I and θ give the angle between the two orbital planes and the angle between the lines of apsides, respectively:

$$I = \arccos\left[\cos i_m \cos i_s + \sin i_m \sin i_s \cos(\Omega_m - \Omega_s)\right] \quad (3)$$

$$\theta = \arccos[\sin \eta_m \sin \eta_s + \cos \eta_m \cos \eta_s \cos(\gamma_s - \gamma_m)]\,. \quad (4)$$

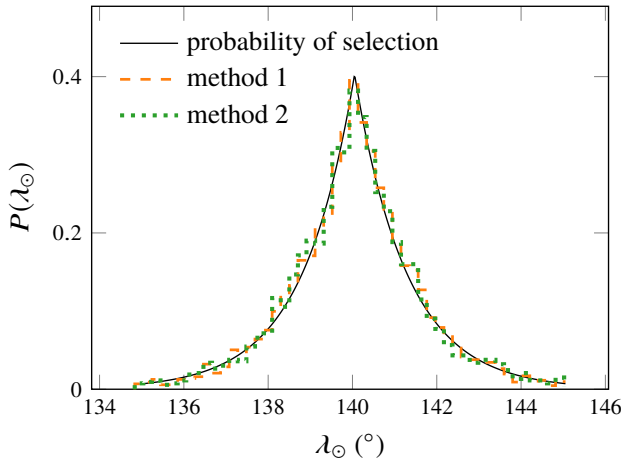

Figure 4 – Solar longitude probability distribution (black line) and normalized histogram of selected simulated solar longitude values for the Perseid meteor shower. Two selection methods are shown: method 1 (dashed orange line) selects meteors based on their radiant and velocity, and method 2 (dotted green line) uses an orbital dissimilarity parameter.

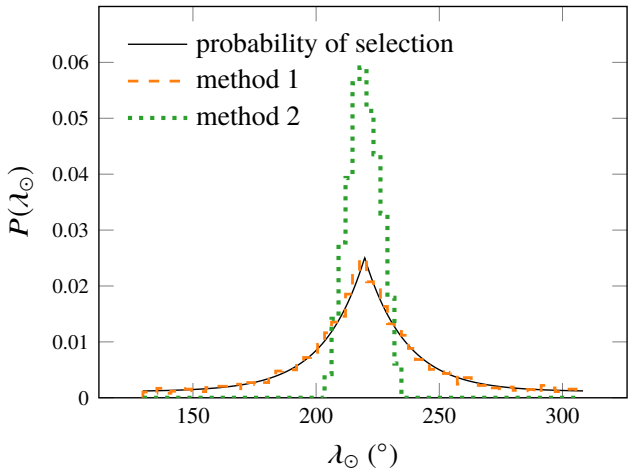

Figure 5 – Solar longitude probability distribution (black line) and normalized histogram of selected simulated solar longitude values for the Southern Taurid meteor shower. Two selection methods are shown: method 1 (dashed orange line) selects meteors based on their radiant and velocity, and method 2 (dotted green line) uses an orbital dissimilarity parameter.

The symbols γ and η give the ecliptic longitude and latitude of each orbit's perihelion, which can be computed as follows:

$$\gamma = \Omega + \arctan(\cos i \tan \omega) \quad (5)$$

$$\eta = \arcsin(\sin i \sin \omega) \quad (6)$$

where ω is the argument of pericenter and Ω is the longitude of the ascending node.

For membership, we require $D < 0.18$ for the Perseids and $D < 0.06$ for the Southern Taurids. Although these cutoff values correspond to 70% shower retrieval according to Galligan (2001), we do not achieve 70% recovery. Instead, this method recovers 52% of Perseids and 25% of Taurids (not including noise meteors). This may be because we have simulated measurement errors larger than those encountered by Galligan (2001) in the AMOR (Advanced Meteor Orbit Radar) data. In general, the shower retrieval thresholds will vary between networks and even between showers; those wishing to optimize their shower member retrieval rate should characterize its dependence on the D cutoff value within their data set (Moorhead, 2016).

3.3 Results

Figures 4 and 5 show the distribution of simulated meteor solar longitudes selected using these two methods. In the case of the Perseids, both methods preserve the activity profile of the shower. However, in the case of the Southern Taurids, the use of an orbital dissimilarity parameter (method 2) significantly alters the shape of the activity profile. In fact, if we attempt to measure B from the distribution labeled "method 2" in Figure 5, we obtain a value of about 0.08, which is between 3 and 4 times the value used to generate the simulated data.

4 Conclusion

We have demonstrated that the use of orbital dissimilarity parameters to select members of a meteor shower can result a shower activity profile that is artificially brief and steep in shape. This effect is not significant for short-to-medium duration showers such as the Perseids, but can be quite significant for long-duration showers such as the Southern Taurids. It will occur for any method that incorporates time, solar longitude, or longitude of the ascending node into a single measure of shower member likelihood. This includes not only the Drummond D, but most other variants (including Southworth & Hawkins, 1963; Jopek, 1993; Valsecchi et al., 1999; Neslusan, 2002; Jopek et al., 2008).

It may be beneficial to preferentially omit meteors that occur far from the peak; for instance, the use of the Drummond D parameter to select Southern Taurids from our simulated date retrieves 25% of simulated Taurids, but only 2% of the simulated noise. Thus, a D-parameter-based selection method can reduce the quantity of sporadic interlopers and perhaps improve the calculation of an average orbit. It is therefore important to tailor one's shower selection method to one's end goal.

One can sidestep the bias discussed here in one of two ways. The first solution is to disregard time, solar longitude, or longitude of ascending node when assessing shower membership. For instance, the wavelet coefficient presented by Brown et al. (2008) uses only (Sun-centered ecliptic) radiant and velocity to detect showers. Their search is conducted once per degree of solar longitude and similar wavelet peaks on adjacent days are linked afterwards. As a result, temporal clustering does not enter into the initial selection method and will not affect the activity profile.

A second, equivalent approach is to use a set of reference shower orbits (or radiants and velocities) instead of a single, static orbit. If the solar longitude or longitude of ascending node of the reference orbits varies over time in a manner that accurately traces the shower's behavior, and similarity to any of these reference orbits

qualifies the meteor as a shower member, the temporal bias we've discussed will be avoided. An example of this approach can be found in Jenniskens et al. (2018), who generated a "look-up table" that describes how shower elements drift over time.

References

Brown P., Weryk R. J., Wong D. K., and Jones J. (2008). "A meteoroid stream survey using the Canadian Meteor Orbit Radar. I. Methodology and radiant catalogue". *Icarus*, **195**, 317–339.

Brown P., Wong D. K., Weryk R. J., and Wiegert P. (2010). "A meteoroid stream survey using the Canadian Meteor Orbit Radar. II: Identification of minor showers using a 3D wavelet transform". *Icarus*, **207:1**, 66–81.

Campbell-Brown M. D. and Jones J. (2006). "Annual variation of sporadic radar meteor rates". *Monthly Notices of the Royal Astronomical Society*, **367**, 709–716.

Cooke W. J. and Moser D. E. (2012). "The status of the NASA All Sky Fireball Network". In *Proceedings of the International Meteor Conference, 30th IMC, Sibiu, Romania, 2011.* pages 9–12.

Drummond J. D. (1981). "A test of comet and meteor shower associations". *Icarus*, **45**, 545–553.

Dubietis A. and Arlt R. (2002). "The current Delta-Aurigid meteor shower". *WGN, Journal of the International Meteor Organization*, **30:5**, 168–174.

Galligan D. P. (2001). "Performance of the D-criteria in recovery of meteoroid stream orbits in a radar data set". *Monthly Notices of the Royal Astronomical Society*, **327**, 623–628.

Jenniskens P. (1990). "Meteor Stream Activity Profiles From Naked Eye Counts". In Lagerkvist C. I., Rickman H., and Lindblad B. A., editors, *Asteroids, Comets, Meteors III.* page 535.

Jenniskens P. (1994). "Meteor stream activity I. The annual streams". *Astronomy & Astrophysics*, **287**, 990–1013.

Jenniskens P., Baggaley J., Crumpton I., Aldous P., Pokorny P., Janches D., Gural P. S., Samuels D., Albers J., Howell A., Johannink C., Breukers M., Odeh M., Moskovitz N., Collison J., and Ganju S. (2018). "A survey of southern hemisphere meteor showers". *Planetary & Space Science*, **154**, 21–29.

Jopek T. J. (1993). "Remarks on the meteor orbital similarity D-criterion". *Icarus*, **106**, 603–607.

Jopek T. J., Rudawska R., and Bartczak P. (2008). "Meteoroid Stream Searching: The Use of the Vectorial Elements". *Earth Moon and Planets*, **102:1-4**, 73–78.

McBride N. (1997). "The importance of the annual meteoroid streams to spacecraft and their detectors". *Advances in Space Research*, **20**, 1513–1516.

McDonnell T., McBride N., Green S. F., Ratcliff P. R., Gardner D. J., and Griffiths A. D. (2001). *Near Earth Environment*, pages 163–231. Berlin: Springer.

Moorhead A. V. (2016). "Performance of D-criteria in isolating meteor showers from the sporadic background in an optical data set". *Monthly Notices of the Royal Astronomical Society*, **455**, 4329–4338.

Moorhead A. V., Cooke W. J., and Campbell-Brown M. D. (2017). "Meteor shower forecasting for spacecraft operations". *7th European Conference on Space Debris*, **7**, 11.

Moorhead A. V., Egal A., Brown P. G., Moser D. E., and Cooke W. J. (2019). "Meteor shower forecasting in near-Earth space". *Journal of Spacecraft and Rockets*, **56**, 1531–1545.

Neslusan L. (2002). "A Sketch of an Orbital-Momentum-Based Criterion of Diversity of Two Keplerian Orbits". In Pretka-Ziomek H., Wnuk E., Seidelmann P. K., and Richardson D., editors, *Dynamics of Natural and Artificial Celestial Bodies*, volume 81. pages 365–366.

Olech A., Gajos M., and Jurek M. (1999). "Alpha Cygnids – a possible July minor meteor shower". *Astronomy & Astrophysicss*, **135**, 291–297.

SonotaCo (2009). "A meteor shower catalog based on video observations in 2007-2008". *WGN, Journal of the International Meteor Organization*, **37**, 55–62.

Southworth R. B. and Hawkins G. S. (1963). "Statistics of meteor streams". *Smithsonian Contributions to Astrophysics*, **7**, 261–285.

Valsecchi G. B., Jopek T. J., and Froeschle C. (1999). "Meteoroid stream identification: a new approach – I. Theory". *Monthly Notices of the Royal Astronomical Society*, **304**, 743–750.

Handling Editor: Denis Vida
This paper has been typeset from a LaTeX file prepared by the author.

Legendary meteor showers: Studies on Harvard photographic results

Masahiro Koseki[1]

We studied 7 out of 28 showers found from the graphical reduction of meteors (McCrosky and Posen, 1961), excluding well known ones. It is clear that small data samples misled researchers to recognize a meteor shower especially near the Antihelion (ANT) area, although 2529 photographic meteors were thought to be a large sample. The ι-Aquarids (southern branch) and δ-Arietids are chance associations of sporadics. The α-Virginids are called now HVI (h-Virginids) and not AVB (alpha-Virginids) in the IAUMDC meteor shower database (SD, 2018; this study used Jan 13 20:35:17 2018 version). The ι-Aquarids (northern branch) are identified with the NIA in the SD, but the NIAs listed in the SD are not the same as the original shower: entries 3, 4 and 7 of NIA in the SD form the new ω-Piscids. Virginids are identical to EVI – but EVI meteors in the Harvard catalogue are mostly overlooked; Virginids include only one EVI meteor and consist mainly of sporadics. The southern Arietids – originally listed as number 18 – are now part of the STA complex which consists of two branches at least: a primary activity around $\lambda_s = 220°$ and a secondary near $\lambda_s = 200°$. The STA in the SD is a conglomerate of such branches and does not represent the real activity; the ecliptic longitude of the Sun at the peak shower activity of STAs in SD are widely spread between $\lambda_s = 196°$ and 224°. We should be careful to propose or to identify meteor showers based only on D-criterions without considerations on the background activities/sporadics. There are many unreliable examples not only in legendary showers but in the recent SD.

Received 2019 September 24

1 Introduction

Whipple and Hawkins (1959, p. 545) presented the original form of the shower database, SD. We have known several new photographic meteor showers detected from Harvard Super-Schmidt results and, thenceforth, observed meteor showers through their views for a long time. They numbered meteor showers – which we use until now – and gave these numbers for the classifications in their meteor data. McCrosky and Posen (1961) published photographic data from the graphical reduction and identified 28 showers:
1. α-Capricornids, 2. Southern Taurids, 3. ι-Aquarids (southern branch), 4. Geminids, 5. δ-Aquarids (southern branch), 6. Lyrids, 7. Perseids, 8. Orionids, 9. Draconids. 10. Quadrantids, 11. Virginids, 12. κ-Cygnids, 13. Leonids, 14. χ-Orionids, 15. Ursids, 16. σ-Hydrids, 17. Northern Taurids, 18. Southern Arietids, 19. Monocerotids, 20. Coma Berenicids, 21. α-Virginids, 22. Leo Minorids, 23. ε-Geminids, 24. μ-Pegasids, 25. δ-Arietids, 26. δ-Aquarids (northern branch), 27. κ-Serpentids, 33. ι-Aquarids (northern branch).

These numbers are inherited by the current IAUMDC (2018) meteor shower database (SD), though some are replaced: 11. Virginids with η-Virginids (EVI), 18. Southern Arietids with Andromedids and 25. δ-Arietids with Northern October δ-Arietids and, finally, the 24. μ-Pegasids are deleted.

There are many well observed and studied meteor showers but some are less known; 3. ι-Aquarids (southern branch), 11. Virginids, 14. χ-Orionids, 18. Southern Arietids, 21. α-Virginids, 25. δ-Arietids, 27. κ-Serpentids, 33. ι-Aquarids (northern branch). We know the 14. χ-Orionids which are listed in the Harvard table but not mentioned in the list of "orbital and physical parameters of 2529 double-station meteors" (McCrosky and Posen, 1961); the χ-Orionids are classified as "group members: 256/ORN, 257/ORS" in the SD. Therefore, we investigate seven legendary meteor showers mentioned above using video meteor data of the SonotaCo network (SonotaCo, 2009).

2 Legendary Showers

2.1 ι-Aquarids (southern branch)

The ι-Aquarids (southern branch) are now called "Southern ι-Aquariids" (SIA) – spelled *Aquariids* while the former *Aquarids* is no longer used. The ι-Aquarids (southern branch) had been thought to be more ac-

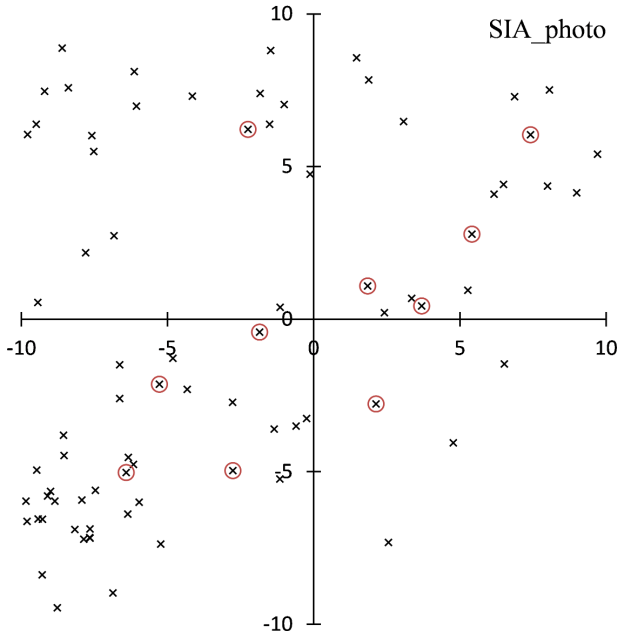

Figure 1a – Photographic radiant distribution during the supposed period of ι-Aquarids (southern branch) activity $98\overset{\circ}{.}2 < \lambda_s < 149\overset{\circ}{.}7$. The plot is centered at the median point of the ι-Aquarids (southern branch) at $(\lambda - \lambda_s, \beta) = (198\overset{\circ}{.}3, -1\overset{\circ}{.}7)$.

[1]The Nippon Meteor Society (NMS), 4-3-5 Annaka-shi, Annaka Gunma-ken, 379-0116 Japan.
Email: geh04301@nifty.ne.jp

IMO bibcode WGN-475-koseki-showers
NASA-ADS bibcode 2019JIMO...47..139K

Table 1a – ι-Aquarids (southern branch) meteors listed by McCrosky and Posen (1961).

Code	λ_s	$\lambda - \lambda_s$	β	V_g	x	y	r	Note
H3-4199	98.3	200.5	4.6	30.32	−10.7	3.9	11.4	?
H3-3355	117.3	196.4	−0.6	32.58	−6.6	−1.2	6.7	
H3-8110	119.0	190.9	4.4	29.22	−1.0	3.7	3.9	
H1-3406	123.7	192.9	1.1	34.4	−3.1	0.5	3.1	
H3-3407	123.9	194.6	−1.2	33.16	−4.8	−1.9	5.1	
H3-8307	136.0	196.2	−4.4	33.99	−6.3	−5.1	8.1	
H1-3619	145.7	203.6	−3.8	35.4	−13.7	−4.5	14.4	
H1-8624	147.7	200.2	−2.1	37.4	−10.3	−2.7	10.7	
H1-3658	148.7	204.7	−6.7	37.4	−14.8	−7.4	16.6	
H3-3784	149.7	201.1	−6.6	35.56	−11.2	−7.3	13.4	
min	98.3	190.9	−6.7	29.2				
max	149.7	204.7	4.6	37.4				
median	129.9	198.3	−1.7	34.2				
mean	131.0	198.1	−1.5	33.9				
sd	16.4	4.4	3.8	2.6				

Note: Wright et al. (1957) wrote H3-4199 is a very doubtful member and added H3-8106 as another doubtful member.

Table 1b – Observations of ι-Aquarids (southern branch).

Code	α	δ	V_g	λ_s	$\lambda - \lambda_s$	β	e	q	i	ω	Ω	Stream
K1-90	328.7	−17.8	33.0	127.7	197.0	−4.8	0.88	0.26	8.0	126.0	307.7	S ι-Aquariids
S2-47	336.0	−8.8	28.8	136.9	197.6	1.1	0.836	0.277	1.4	307.7	136.7	Southern ι-Aquarids
S3-137	343.6	−2.9	24.5	138.0	205.8	3.7	0.76	0.25	4.4	319.2	137.9	Southern ι-Aquarids
L1-60	320.7	−14.8	35	124.7	193.7	0.5	0.925	0.27	0.0	70.7	355.5	Southern ι-Aquarids
L1-110	348.7	−9.7	41	142.5	203.3	−4.5	0.959	0.119	12.6	143.9	322.5	Southern ι-Aquarids

Note: The inclination of L1-60 is very small ($i = 0\overset{\circ}{.}0$) and the strict conversion B1950.0 to J2000.0 led us to curious results ($\omega = 70\overset{\circ}{.}7$ and $\Omega = 355\overset{\circ}{.}5$) but the activity could remain at $\lambda_s = 124\overset{\circ}{.}7$.

Table 1c – Meteor showers in SD possibly concerning to ι-Aquarids (southern branch) shown in Figure 1a.

Code	λ_s	$\lambda - \lambda_s$	β	V_g	x	y	r
0689TAC01	108.8	190.1	3.4	28.9	8.0	5.0	9.5
0179SCA00	110	199.6	3.5	26.9	−1.5	5.1	5.3
0179SCA01	118	200.5	4.6	34.1	−2.4	6.3	6.7
0689TAC00	121	188.9	2.2	28.2	9.3	3.8	10.0
0921JLC00	124.7	203.6	3.8	37.3	−5.4	5.5	7.7
0003SIA02	129.5	200.1	−3.3	30.5	−2.0	−1.6	2.6
0005SDA07	129.7	207.4	−7.9	39.4	−9.3	−6.3	11.2
0003SIA00	131.7	199.7	−3.5	33.8	−1.6	−1.8	2.4
0003SIA01	131.7	203.1	−6.3	34.8	−4.9	−4.6	6.8
0003SIA03	135.6	198.7	−3.6	28.9	−0.6	−1.9	2.0
0640AOA00	137	206.8	−8.7	38.2	−8.6	−7.1	11.1
0026NDA00	139	207.1	6.4	40.5	−8.9	8.1	12.0
0026NDA02	139.6	199.8	3.6	42.3	−1.7	5.3	5.5
0026NDA04	140	208.0	6.7	38.3	−9.9	8.3	12.9
0342BPI00	140	208.0	6.7	38.3	−9.9	8.3	12.9
0640AOA01	140.5	206.6	−8.7	37.8	−8.4	−7.1	11.0
0026NDA01	140.7	206.0	6.3	39.78	−7.8	7.9	11.1
0033NIA04	142	190.9	2.3	29.4	7.2	4.0	8.2
0473LAQ01	145.3	195.2	2.7	31.12	2.9	4.4	5.2
0505AIC00	145.4	207.8	−7.5	37.24	−9.6	−5.9	11.3
0026NDA07	146.5	207.3	7.0	38.1	−9.1	8.7	12.6
0508TPI01	146.5	207.3	7.0	38.1	−9.1	8.7	12.6
0026NDA09	146.6	207.4	7.0	38.2	−9.2	8.6	12.6
0026NDA06	147	207.3	6.9	39	−9.1	8.6	12.5
0508TPI00	147	207.3	6.9	39	−9.1	8.6	12.5
0473LAQ02	147.5	199.7	4.1	32.2	−1.5	5.7	6.0
0473LAQ00	147.6	194.0	1.9	30.6	4.1	3.5	5.4
0033NIA05	148	199.3	4.1	31.3	−1.2	5.8	5.9

Note: Code is assembled by IAUNo.+IAUcode+AdNo;
e.g., 0003SIA00 is the first entry of the third shower in the SD named SIA.

tive than the ι-Aquarids (northern branch: now Northern ι-Aquariids, NIA) – see Wright et al. (1957) – and listed as an "established shower" in the early SD. Table 1a shows the summary data of meteors classified as ι-Aquarids (southern branch) members (McCrosky & Posen, 1961) and their radiant distribution is shown in Figure 1a. Figure 1a is centered at the median values of Table 1a and the y-axis runs through $\lambda - \lambda_s = 198\overset{\circ}{.}1$ (scales are in degrees). Circled crosses are meteors listed in Table 1a and x, y and r in the table gives each positions in the figure. Abbreviations of the meteor code in Table 1a are the same ones of Koseki (2009); several meteor data in H1 are replaced by more accurate data indicated by H3.

Meteors classified as ι-Aquarids (southern branch) were observed within a very long period (min and max of Table 1a; though H3-4199 is doubted by the authors) and are distributed over a long elongated area top right to bottom left with several other possibly associated meteors (Figure 1a). It seems to be natural

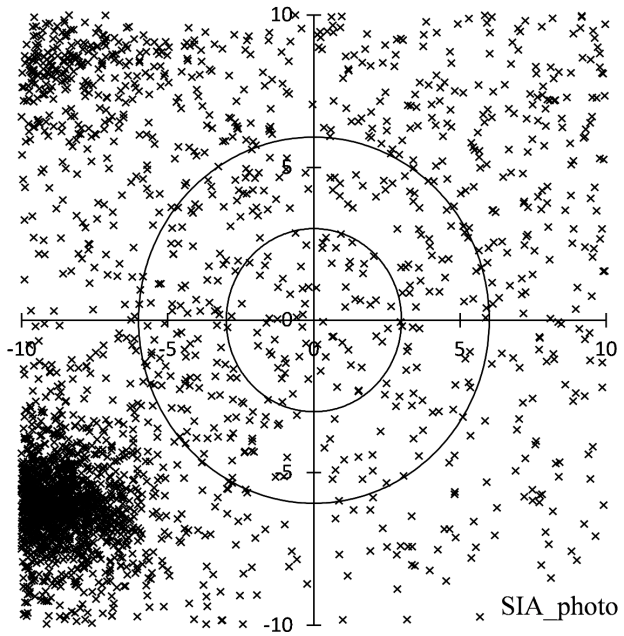

Figure 1b – Video (SonotaCo net) radiant distribution plotted in the same manner as Figure 1a.

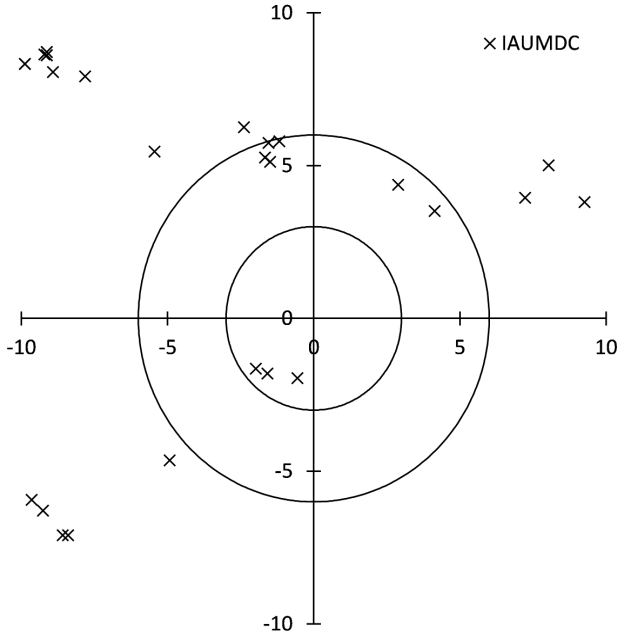

Figure 1c – The distribution of SD meteor shower radiant plotted similar to Figure 1a.

there may be some meteor activity(-ies) and several researchers found ι-Aquarids (southern branch) activities (Table 1b; see Koseki (2009) for the abbreviations of the code in Table 1b).

However, we cannot detect such activities by recent video observations (Figure 1b). The center is placed at the same point as Figure 1a and the period is the same ($98.2 < \lambda_s < 149.7$) as well. The SD lists many meteor activities from this area during the same period (Figure 1c and Table 1c) and the SD has four entries of SIA; they are shown as 0003SIA00 to 03 in Table 1c. Figures 1b and 1c clearly represent SDA (lower left) and NDA (upper left) but there is no clear meteor activity around SIA, though the SIAs of the SD are located around the center. Perhaps the ι-Aquarids (southern branch) represent possible past meteor activities observed in the period 1950–70. It seems to be better to move SIA to the list of historical records.

2.2 Virginids

The name "Virginids" is troublesome: Hoffmeister (1948) designated widely spread ecliptic meteor activities in spring as "Virginids". Many researchers and observers called meteor activities from March to May as "Virginids" arbitrarily. Harvard's "Virginids" is very conspicuous in this respect: it is active during a few days only (Table 2a). The radiant distribution shown in Figure 2a is, therefore, drawn in an extended range $350° < \lambda_s < 360°$. The SD identifies this activity with the η-Virginids (EVI), though EVI is located at a slightly higher latitude (Figures 2b and 2c). Comparing these three figures, we notice that Figure 2a shows that only H1-6798 belongs to EVI; the other 4 meteors are probably sporadic. It is interesting to know why the Harvard researchers missed the upper right concentration in Figure 2a), which in fact is EVI. If we select possible EVI meteors from the Figure 2a, we find H1-6798 as the original "Virginids" while the other 9 meteors are possibly EVI meteors (although H1-6849 is too slow for EVI; Table 2b). If we reject it and use only the H1 and H3 sources, which are Super-Schmidt meteors, there remain only 4 meteors including H1-6798. Moreover, the other 3 meteors occur later than the activity period of "Virginids" (see the values of min and max of λ_s in Table 2a). It is natural that researchers at that time did not recognize the concentration suggesting EVI activity. From the 'Virginids' case we should learn that it is very important to have a large enough amount of data available in order to distinguish meteor activity from ANT background.

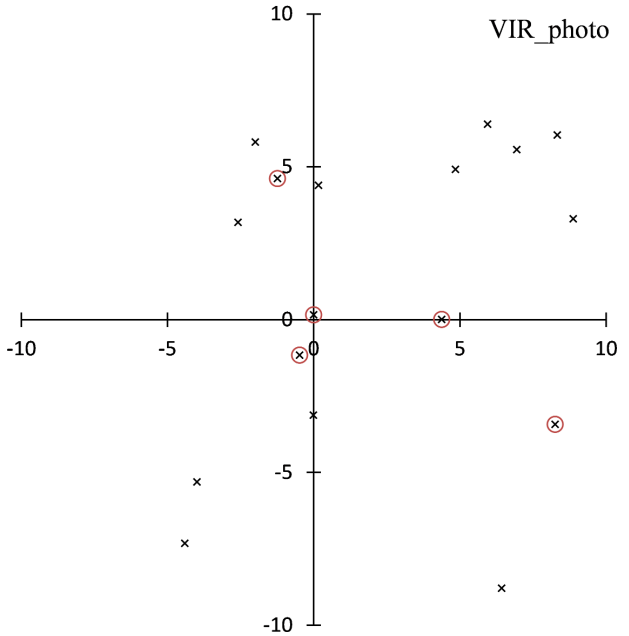

Figure 2a – Photographic meteors during "Virginid" activity $350° < \lambda_s < 360°$. The graph is centered at $(\lambda - \lambda_s, \beta) = (189\overset{\circ}{.}8, 0\overset{\circ}{.}6)$.

Table 2a – "Virginids" listed by McCrosky and Posen (1961).

Code	λ_s	$\lambda - \lambda_s$	β	V_g	x	y	r
H1-6786	351.7	190.3	−0.5	26.8	−0.5	−1.2	1.3
H1-6798	351.7	191.1	5.3	30.6	−1.2	4.6	4.8
H1-6807	351.7	185.5	0.6	25.8	4.4	0.0	4.4
H1-6816	352.7	189.8	0.8	25.4	0.0	0.2	0.2
H1-6822	352.7	181.6	−2.8	24.3	8.3	−3.4	8.9
min	351.7	181.6	−2.8	24.3			
max	352.7	191.1	5.3	30.6			
median	351.7	189.8	0.6	25.8			
mean	352.1	187.7	0.7	26.6			
sd	0.5	3.6	2.6	2.2			

Table 2b – Possible EVI meteors in Figure 2a. H5-1158 is added after the period though.

Code	λ_s	$\lambda - \lambda_s$	β	V_g	x	y	r
H1-6798	351.7	191.1	5.3	30.6	−1.2	4.6	4.8
H1-6869	353.7	180.9	3.9	25.8	8.9	3.3	9.5
H1-6849	353.7	191.8	6.5	17.4	−2.0	5.8	6.1
H5-1934	357.9	189.7	5.0	29.2	0.2	4.4	4.4
H3-6949	358.2	182.9	6.2	24.97	6.9	5.6	8.9
O1-40	358.5	185.0	5.6	26	4.9	4.9	6.9
H6-41029	358.7	183.9	7.0	22.7	5.9	6.4	8.7
H5-828	359.5	181.5	6.7	31	8.3	6.0	10.3
H1-7019	359.7	192.4	3.8	31.4	−2.6	3.2	4.1
H5-1158	0.7	183.9	6.1	28.4	5.9	5.4	8.0
min	351.7	180.9	3.8	17.4			
max	360.7	192.4	7.0	31.4			
median	358.3	184.4	5.8	27.2			
mean	357.2	186.3	5.6	26.7			
sd	2.9	4.2	1.0	4.1			

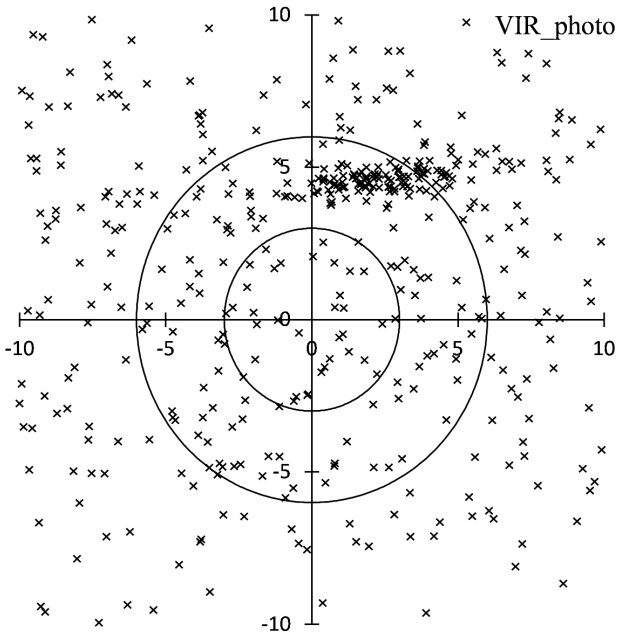

Figure 2b – Video meteor radiants plotted in the same way as in Figure 2a.

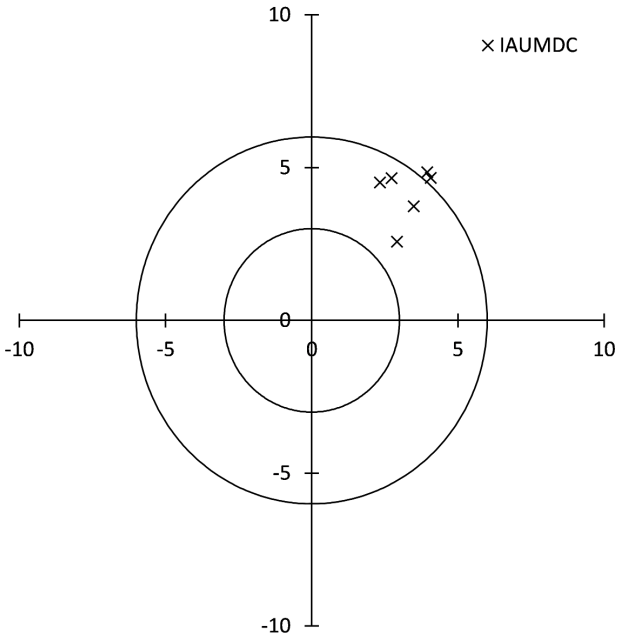

Figure 2c – Data of SD showers plotted similar to Figure 2a.

2.3 Southern Arietids

Harvard's number 18 were the Southern Arietids which may be distinguishable from the Southern Taurids (STA). (Entry number 18 of the current SD is assigned to the Andromedids, AND.) Whipple (1940) found that the "Taurids" have two components, namely the Southern and Northern branches and the former might be divided to earlier and later activities. The name "Southern Arietids" is inherited from Whipple's suggestion. The author confirmed Whipple's idea (Koseki, 2012), though the activities of "Taurids" are very complex. It is worth to restudy the "Southern Arietids" using photographic and video data.

Table 3a gives the "Southern Arietids" listed in the H1 catalogue, though some of them are replaced by their more precise data, that is, H2 and H3. Figure 3a shows their radiant distribution with photographic meteors recorded within the same period (between min and max of λ_s in Table 3a). Meteors of the 'Southern Arietids' are well concentrated around the center with many other photographic radiants; the result of video observations (Figure 3b) is very similar to the photographic results. Figure 3c represents the distribution

Table 3a – Southern Arietids listed by McCrosky and Posen (1961).

Code	λ_s	$\lambda - \lambda_s$	β	V_g	x	y	r
H1-8971	196.7	197.9	−4.0	27	−2.5	0.4	2.5
H1-4764	200.7	198.9	−4.7	29.1	−3.5	−0.2	3.5
H2-4819	201.6	201.8	−3.6	29.7	−6.5	0.8	6.5
H1-4830	201.7	199.1	−4.1	33.1	−3.7	0.4	3.8
H1-9077	201.7	197.9	−4.7	25.9	−2.5	−0.2	2.5
H1-4862	203.7	195.5	−5.6	28.8	−0.2	−1.2	1.2
H1-4883	204.7	194.9	−4.7	29.8	0.5	−0.2	0.5
H1-4907	206.7	195.4	−3.4	29.1	0.0	1.1	1.1
H2-4912	206.5	191.3	−4.0	26.8	4.1	0.5	4.1
H1-4975	208.7	191.2	−3.7	25.9	4.2	0.7	4.2
H1-5115	209.7	193.9	−4.9	28.7	1.4	−0.5	1.5
H3-5176	210.6	193.5	−4.5	28.62	1.8	0.0	1.8
H3-5195	210.7	190.9	−4.6	27.05	4.5	−0.1	4.5
min	196.7	190.9	−5.6	25.9			
max	210.7	201.8	−3.4	33.1			
median	204.7	195.4	−4.5	28.7			
mean	204.9	195.5	−4.4	28.4			
sd	4.2	3.3	0.6	1.9			

Table 3b – Meteor showers in SD possibly concerning to Harvard's 'Southern Arietids'.

Code	λ_s	$\lambda - \lambda_s$	β	V_g	x	y	r
0028SOA02	197.7	196.8	−4.4	28.9	−1.4	0.1	1.4
0028SOA00	198.5	196.0	−2.6	25.6	−0.6	1.9	2.0
0946TEA00	199.3	203.2	−3.2	34.95	−7.7	1.2	7.8
0237SSA00	202.0	204.4	−2.6	40.5	−9.0	1.8	9.2
0902DCT00	202.1	194.4	−13.2	32.7	1.0	−8.7	8.8
0025NOA01	205.0	196.9	2.5	30.1	−1.5	7.0	7.2
0624XAR00	205.0	195.1	−4.6	28.5	0.3	−0.1	0.3
0025NOA02	205.4	194.7	2.7	28.9	0.7	7.2	7.2
0624XAR01	206.0	194.9	−4.5	28.4	0.5	0.0	0.5
0002STA01	207.6	193.8	−5.2	27.8	1.6	−0.7	1.7

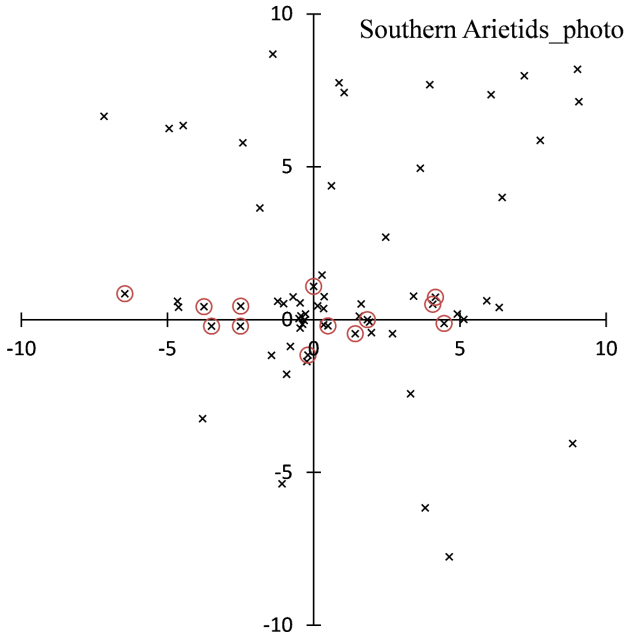

Figure 3a – Photographic meteors during the activity of the "Southern Arietids" in the interval $196.^\circ7 < \lambda_s < 210^\circ7$. The plot is centered at $(\lambda - \lambda_s, \beta) = (195.^\circ4, -4.^\circ5)$.

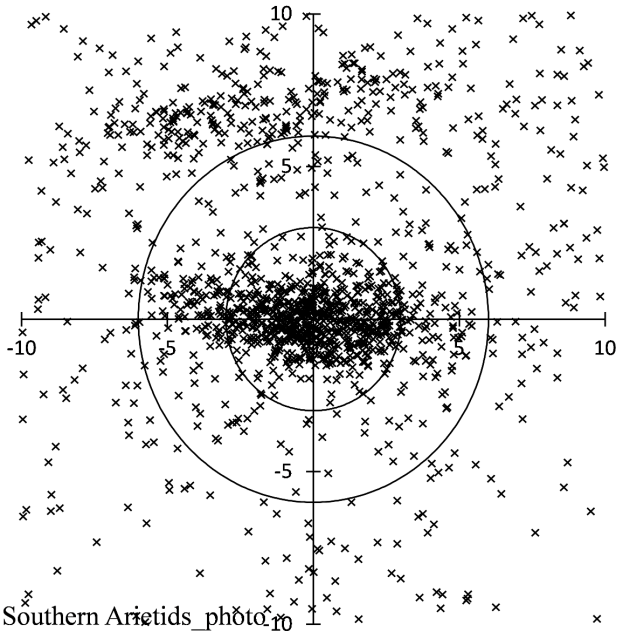

Figure 3b – Video meteor radiants plotted in the same manner as Figure 3a.

of the SD showers; one of STA radiants is located near the center ($x = 1.6$, $y = -0.7$) as listed in Table 3b. The peak activity period for STA listed in the SD is very long: the ecliptic longitude of the Sun at the peak shower activity is in the interval $\lambda_s = 196^\circ$ to 224°. This is not the activity period in total but the maximum of the STA. Some researchers combined all into one but others divided into many smaller parts. Figure 3c represents the unsolved problem whether the "Southern Arietids" are a part of STA or can be divided into smaller parts. We need to study Figure 3c and Table 3b in detail. SOA and XAR are within 3° from the center; NOA is possibly a part of NTA and not necessary to study. There is a remark to the SOA in the SD as "part of 2/STA, member of 299/OAR". OAR (October Arietid Complex) is a curious entry cited from Jenniskens (2006). The basic data including its radiant point are not given and no explanation is added. XAR is one of the micro meteor showers splitting the STA into minia-

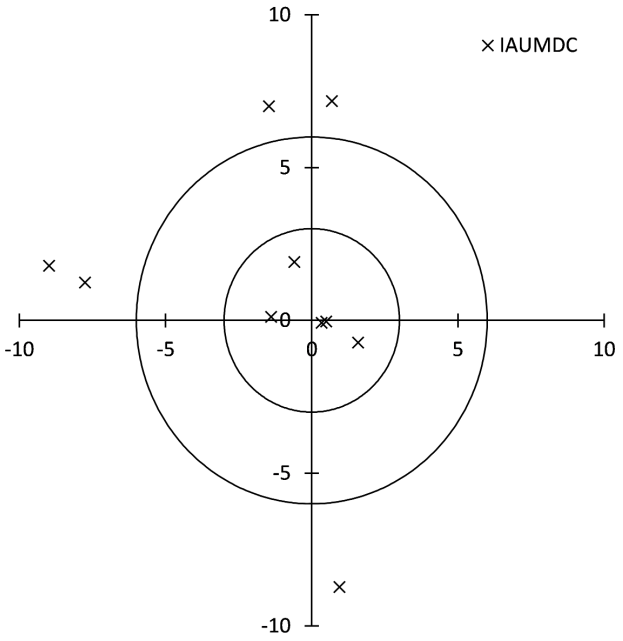

Figure 3c – Data of SD showers plotted similar to Figure 3a.

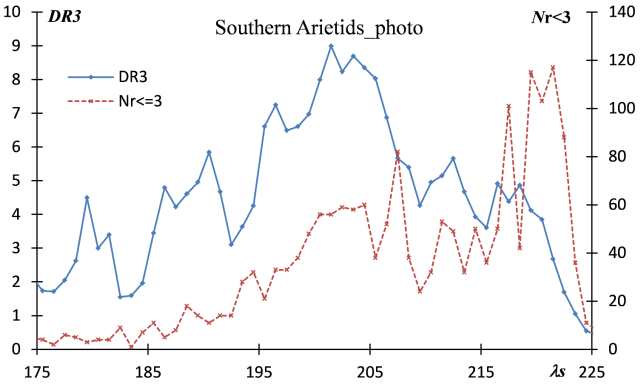

Figure 3d – The estimated activity of the "Southern Arietids". The left axis DR3 represents 3° sliding mean of the radiant density ratios (DR) within 3° to between 3° to 6° from the center of the radiant concentration. The right axis is for the video radiant number within 3° from the center in each solar longitude bin.

tures (Jenniskens et al., 2016) and is supposed to be the core of the "Southern Arietids". It is necessary to study the "Southern Arietids" more precisely whether it is the part of the STA or an independent meteor source.

The author introduced the parameter DR (the radiant density ratios (DR) within 3° to between 3°–6° from the center of the radiant concentration, Koseki (2019a)). DR is useful to figure out the activity profile of a meteor shower. Figure 3d clarifies the independency of "Southern Arietids" from the STA. It is not clear from the raw observed number (Nr < 3), but the parameter DR shows clearly the activity profile. The raw radiant number tends to increase to the maximum of the STA, but DR decreases after its maximum. If we test the STA by this method, there would be a clear gap between the "Southern Arietids" and the STA. This is subject of a detailed study on the validity of DR to several showers which is under preparation and to be published in a forthcoming issue of *WGN* (Koseki, 2019b).

This supports that the "Southern Arietids" should be kept in the SD. But the 3-character-code becomes inconvenient now: ARI (Daytime Arietids) is used already, and SAR (September μ-Arietids), too. It is necessary to introduce a provisional designation like for asteroids and to assign an IAU number and 3-character-code only for established showers.

2.4 α-Virginids

The designation α-Viginids was initially used by McCrosky and Posen (1959) for Virginid activity in early May. Harvard's α-Viginids describe a somewhat different activity from the SD and, moreover, SD's AVB

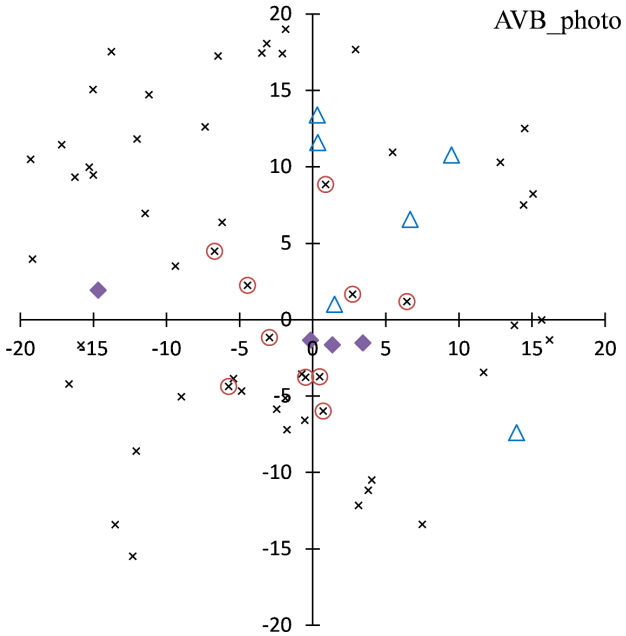

Figure 4a – Harvard's α-Viginid meteors (circled crosses) with AVBs (triangles) and HVIs (diamonds) of the SD. This figure is extended to 20° in the x and y axes and plotted for the period $35° < \lambda_s < 55°$.

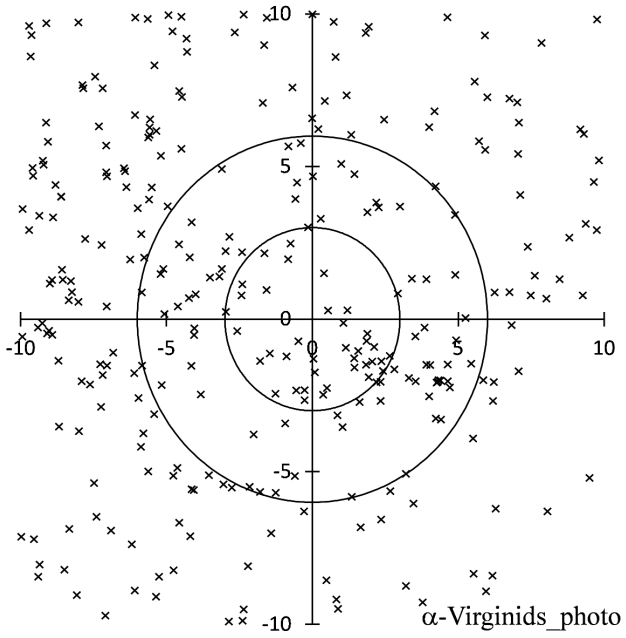

Figure 4b – Video meteor radiants plotted with the same manner as Figure 4a.

Table 4a – α-Viginid meteors listed by McCrosky and Posen (1961).

Code	λ_s	$\lambda - \lambda_s$	β	V_g	x	y	r
H1-11786	40.7	175.7	4.7	22	−6.7	‘ 4.5	8.1
H1-11824	42.7	173.5	2.5	20.7	−4.4	2.2	5.0
H1-11878	43.7	174.8	−4.1	17.1	−5.8	−4.4	7.2
H1-11912	44.7	169.5	−3.5	23.3	−0.5	−3.8	3.8
H1-11949	45.7	168.1	9.1	20	0.9	8.8	8.9
H1-11962	45.7	168.3	−5.7	17.9	0.7	−6.0	6.0
H3-7494	46.1	172.0	−0.9	18.39	−3.0	−1.2	3.2
H2-7514	47.0	166.3	1.9	17	2.7	1.7	3.2
H1-7563	47.7	162.6	1.4	17.4	6.4	1.2	6.5
H1-7593	48.7	168.5	−3.5	16.8	0.5	−3.7	3.8
min	40.7	162.6	−5.7	16.8			
max	48.7	175.7	9.1	23.3			
median	45.7	169.0	0.2	18.1			
mean	45.3	169.9	0.2	19.1			
sd	2.3	3.9	4.4	2.2			

Table 4b – AVB and a related meteor shower HVI in the SD.

Code	λ_s	$\lambda - \lambda_s$	β	V_g	x	y	r
0021AVB00	28	155.0	−7.1	17.6	13.8	−7.4	15.7
0021AVB01	21.7	159.4	10.9	16.8	9.3	10.8	14.3
0021AVB02	28.9	167.5	1.2	16.6	1.4	1.0	1.7
0021AVB03	31.8	162.3	6.8		6.5	6.6	9.3
0021AVB04	32.0	168.7	11.8	18.8	0.2	11.6	11.6
0021AVB05	30.0	168.7	13.6	18.9	0.2	13.4	13.4
0343HVI00	39.0	167.6	−1.4	18.7	1.2	−1.7	2.1
0343HVI01	32	183.7	2.1	24.1	−14.8	1.9	14.9
0343HVI02	38.0	169.2	−1.1	17.2	−0.3	−1.4	1.4
0343HVI03	40.6	165.6	−1.3	18.0	3.3	−1.5	3.6

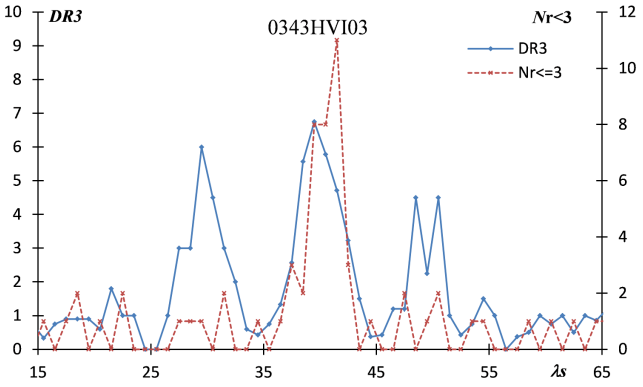

Figure 4c – The estimated activity profile of 0343HVI03.

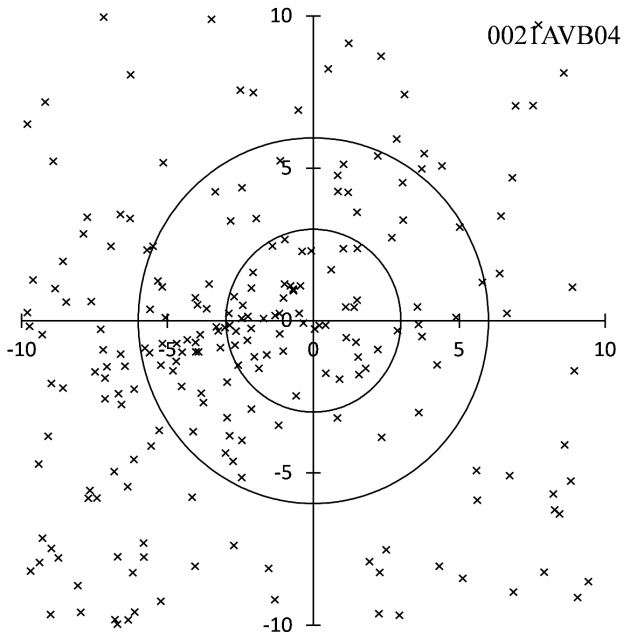

Figure 4d – Radiant distribution of video meteors centered at 0021AVB04 in the period $15° < \lambda_s < 35°$.

seems to be a conglomerate of sporadics and other meteor showers (Koseki, 2016).

Table 4a shows the α-Viginid meteors listed by McCrosky and Posen (1961) and we can realize the activity period starts not earlier than $\lambda_s = 40°$. Figure 4a compares α-Viginid meteor radiants with the AVB's and the HVI's of the SD (Table 4b) and shows clearly that the HVIs' radiants are close to the center except for 0343HVI01. It is also shown clearly by Table 4b that the AVB of the SD occur too early for α-Viginids and the HVI are nearer to the α-Viginids. Obviously, the α-Viginids probably coincide with the HVI and not with the AVB.

Video observations strongly suggest that the HVI is active near the center of α-Viginid radiants (Figure 4b). The group of radiants near the center in Figure 4b represents HVI judging from the radiant distribution of Figure 4a. We can identify α-Viginids with HVI but not AVB in the SD. Figure 4c is the estimated profile for 0343HVI03 similar with Figure 3d and the DR curve reaches its peak around $\lambda_s = 40°$. This suggests that "α-Viginids" might consist of late HVI and sporadics. All AVBs' DR curves suggest that the AVB in the SD is not identical to HVI, that is, not identical to the "α-Viginids".

It is interesting to note that 0021AVB04 and 05 might be a clue to the confusion in AVB. Figures 4d and 4e show the radiant distribution of video meteors around 0021AVB04 and the estimated profile of it, respectively. Both figures indicate clearly that there is a meteor activity. This previously not named shower is independent of the α-Viginids because the radiant point

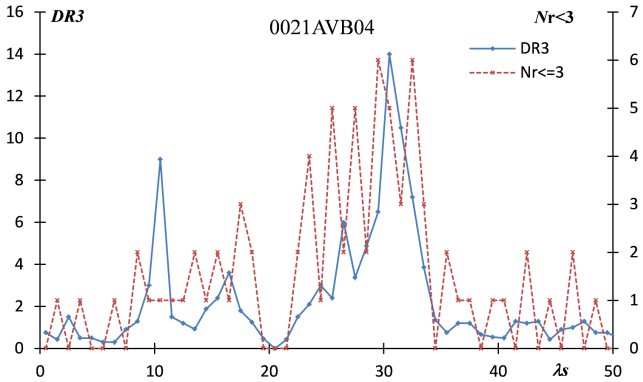

Figure 4e – The estimated activity profile of 0021AVB04.

is 10° north and the peak activity deviates from the α-Viginids about 10° in λ_s. This would justify σ-Virginids as an appropriate designation.

2.5 δ-Arietids

Figure 5a shows the photographic radiant distribution around the "δ-Arietids" and Figure 5b gives the video radiant distribution of the same area. We cannot recognize any meteor activity in this area and in this period. It seems to be natural that the 25th shower δ-Arietids were replaced by Northern October δ-Arietids.

The "δ-Arietids" locate west of ANT where radiants are scarce on the average and, therefore, the radiant distribution might be noticed by researchers then.

Wide spread radiants had been combined into one meteor shower in the 1960-s, σ-Leonids for example (Southworth & Hawkins, 1963). Table 5 shows the summary of "δ-Arietids" with D_{SH} (Southworth & Hawkins, 1963) obtained from the median orbital elements of the "δ-Arietids": $e = 0.70$, $q = 0.90$, $i = 1\overset{\circ}{.}6$, $\omega = 232\overset{\circ}{.}1$, $\Omega = 259\overset{\circ}{.}9$. The "$\delta$-Arietids" might have other members: H1-9895 (0.090), H4-9606b (0.092), H1-5527 (0.125), H1-5752 (0.140), H1-9615 (0.142) within the limits of "δ-Arietids" H1-9486 (0.144). Values in parentheses are D_{SH}s. It seems to be natural there may be enough meteors to recognize a meteor shower activity. But, we cannot confirm such meteor activity by the DR profile and by radiant distribution (Figure 5a). It is noteworthy to state that we might misunderstand a meteor shower activity based on D-criterions only.

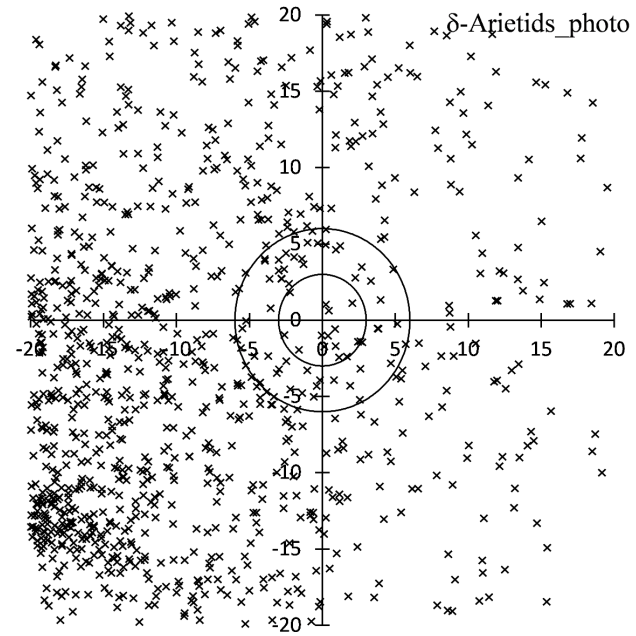

Figure 5b – Video meteor radiants plotted in the same manner as Figure 5a.

2.6 κ-Serpentids

Figure 6a shows the distribution of photographic meteors around the median values (Table 6a) of the κ-Serpentids. We cannot find any clear concentration,

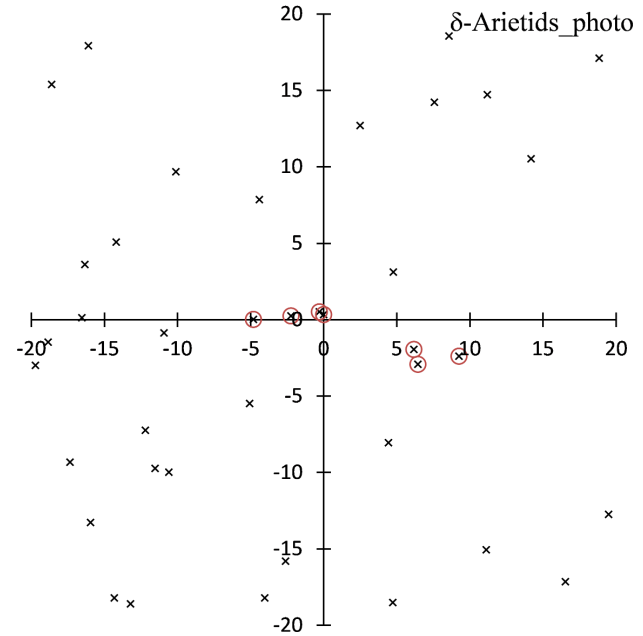

Figure 5a – Photographic meteors during the activity of δ-Arietids in the interval $250° < \lambda_s < 270°$. The figure is centered at $(\lambda - \lambda_s, \beta) = (158\overset{\circ}{.}3, 4\overset{\circ}{.}5)$.

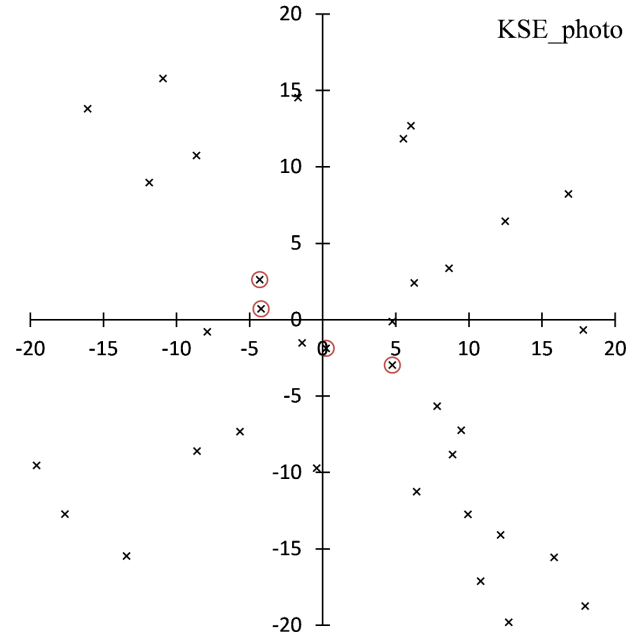

Figure 6a – Photographic meteors during the activity of κ-Serpentids in the interval $10° < \lambda_s < 30°$. The graph is centered at $(\lambda - \lambda_s, \beta) = (209\overset{\circ}{.}2, 34\overset{\circ}{.}3)$.

Table 5 – "δ-Arietids" meteors with D_{SH} calculated from the median "δ-Arietids" orbit.

Code	λ_s	$\lambda - \lambda_s$	β	V_g	x	y	r	D_{SH}
H1-9438	256.7	160.5	4.8	14.8	−2.2	0.2	2.3	0.044
H2-5552	257.8	158.6	5.0	14.7	−0.3	0.5	0.6	0.034
H2-5573	258.8	158.3	4.8	11.6	0.0	0.3	0.3	0.142
H1-9486	259.7	163.1	4.5	12.7	−4.8	0.0	4.8	0.144
H1-5772	261.7	152.1	2.5	12.2	6.2	−2.0	6.5	0.083
H1-5878	261.7	151.8	1.6	14.5	6.4	−2.9	7.1	0.104
H1-5953	262.7	149.0	2.1	12.7	9.3	−2.4	9.6	0.102
min	256.7	149.0	1.6	11.6				
max	262.7	163.1	5.0	14.8				
median	259.7	158.3	4.5	12.7				
mean	259.9	156.2	3.6	13.3				
sd	2.1	4.8	1.4	1.2				

Table 6a – κ-Serpentids listed by McCrosky and Posen (1961).

Code	λ_s	$\lambda - \lambda_s$	β	V_g	x	y	r
H1-10366	11.7	212.2	37.5	42.0	−4.3	2.6	5.0
H1-10389	12.7	212.0	35.6	44.4	−4.2	0.7	4.3
H1-10099	16.7	206.5	33.1	46.5	0.2	−1.9	1.9
H1-7092	17.7	201.2	31.9	46.7	4.8	−3.0	5.6
min	11.7	201.2	31.9	42.0			
max	17.7	212.2	37.5	46.7			
median	14.7	209.2	34.3	45.5			
mean	14.7	208.0	34.5	44.9			
sd	2.5	4.5	2.2	1.9			

Table 6b – Meteor showers in SD possibly concerning to Harvard's κ-Serpentids.

Code	λ_s	$\lambda - \lambda_s$	β	V_g	x	y	r
0517ALO00	15.5	226.9	22.1	55.7	−16.5	−10.9	19.7
0027KSE00	15.7	206.8	35.0	45	2.0	0.7	2.1
0027KSE01	15.7	209.9	33.3	45.01	−0.5	−1.1	1.2
0517ALO01	15.8	226.9	22.4	56.4	−16.4	−10.6	19.5
0841DHE00	19.5	232.1	46.3	49.5	−15.7	13.9	21.0
0027KSE02	20	213.7	36.6	46.7	−3.6	2.3	4.3
0836ABH00	20.3	223.1	44.6	47.5	−9.9	11.0	14.8
0839PSR00	25.1	211.7	34.3	46.3	−2.0	0.0	2.0
0027KSE03	25.9	216.7	38.3	46.9	−5.8	4.2	7.2

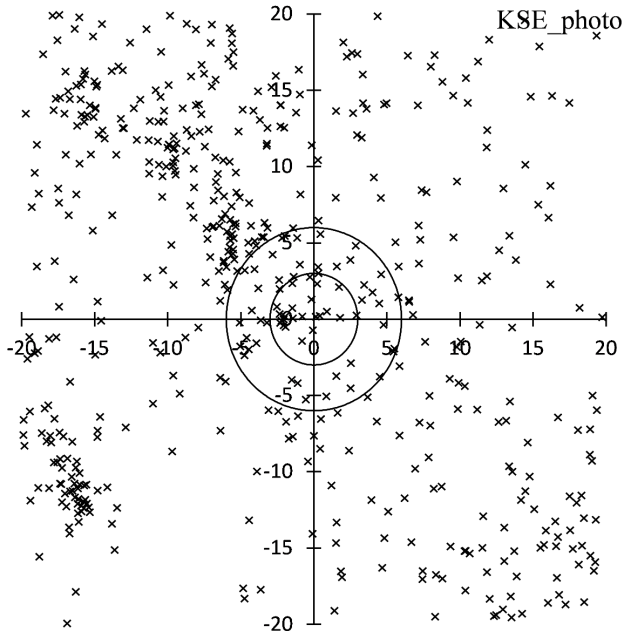

Figure 6b – Video meteor radiants plotted in the same manner as Figure 6a.

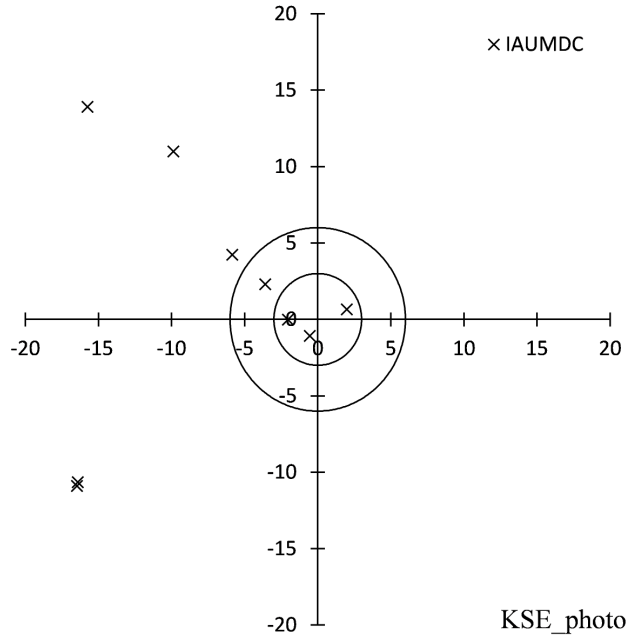

Figure 6c – Data of the SD showers plotted in the same manner as Figure 6a.

though KSE is ranked as "established". Video observations reveal the complex meteor activities in this area and in the period (Figure 6b). Researchers recognized different meteor showers by different manners (Figure 6c and Table 6b). There are 0841DHE00, 0836ABH00, 0027KSE03, 0027KSE02, 0839PSR00, 0027KSE01 and 0027KSE00 in order of top left to the center in Figure 6c.

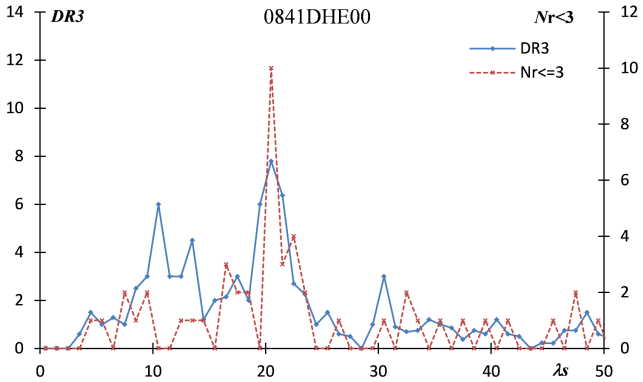

Figure 6d – The estimated activity profile of 0841DHE00.

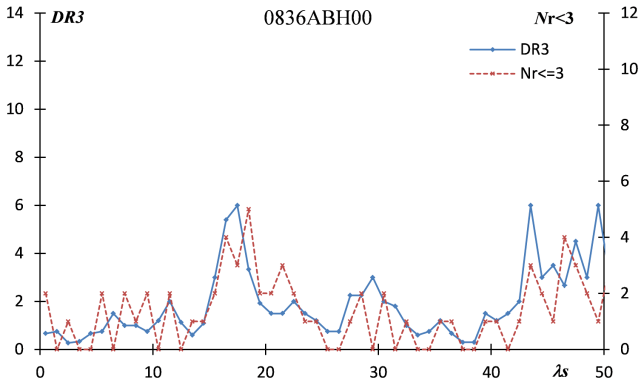

Figure 6e – The estimated activity profile of 0836ABH00.

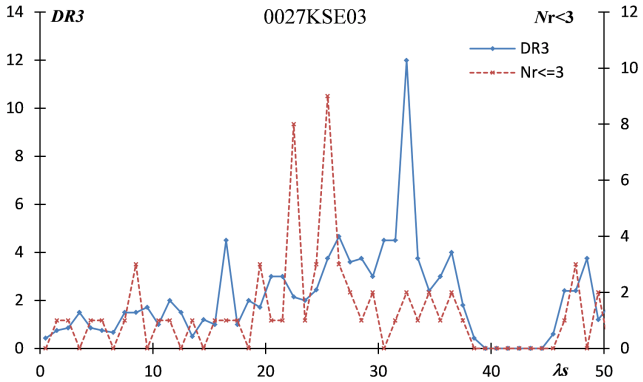

Figure 6f – The estimated activity profile of 0027KSE03.

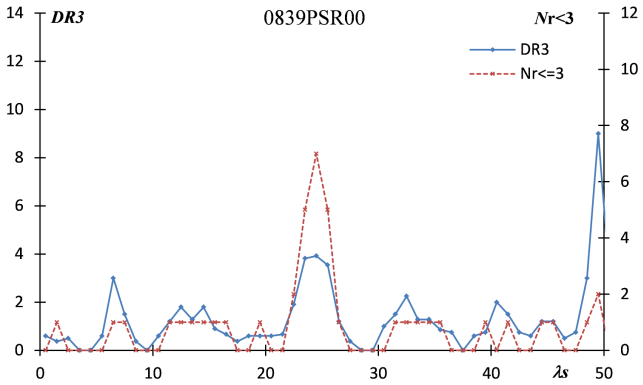

Figure 6g – The estimated activity profile of 0839PSR00.

It might be suggested that there are four groups of radiants in video observations. We could test this supposition by the estimated profile of DR like Figure 3d. We can use 0841DHE00, 0836ABH00, 0027KSE03 and 0839PSR00 as the tentative centers. 0841DHE00 is the farthest of the four from the photographic median position (over 20°) but Figure 6d shows the clearest peak of the four. The first part of its activity period overlaps with the second part of 'κ-Serpentids'.

The peak of 0836ABH00 is the nearest to 'κ-Serpentids' (Figure 6e), though the peak is lower than 0841DHE00 and its position is about 15 degrees from the photographic center. Nr < 3 of 0027KSE03 is over 10 at its peak but DR3 stays low at the peak (Figure 6f). DR3 arises to exceed 10 after λ_s>30, but Nr < 3 is very low and DR3 might be inaccurate then. 0027KSE03 is surrounded by neighbour activities and, therefore, the peak DR3 value might be lowered. If we regard the peak of Nr < 3 represents the real peak, 0027KSE03 would reach its maximum 10 days after "κ-Serpentids".

0839PSR00 has a small but clear peak (Figure 6g) and the nearest of the four to the photographic median. The activity period of 0839PSR00 is not overlapped with "κ-Serpentids" about 10 days later.

We cannot confirm which are enough active to be listed as a candidate of KSE. "KSE" is one of the established showers but "KSE" of the SD lies on the edge of several meteor activities in this area and in the period as shown above. It is necessary to study whether "KSE" is enough to be ranked such position.

2.7 ι-Aquarids (northern branch)

The northern branch of the ι-Aquarids is weaker than southern one in the first study of them (Wright et al., 1957). Figure 7a and Table 7a show ι-Aquarids of Harvard photographic results. Wright et al. (1957) listed these four meteors but McCrosky and Posen (1961) listed H3-3663 (=H1-3663) as a sporadic meteor and H3-3886 (H1-3886) as a member of the STA. If we rejected the latter two meteors, the activity period of

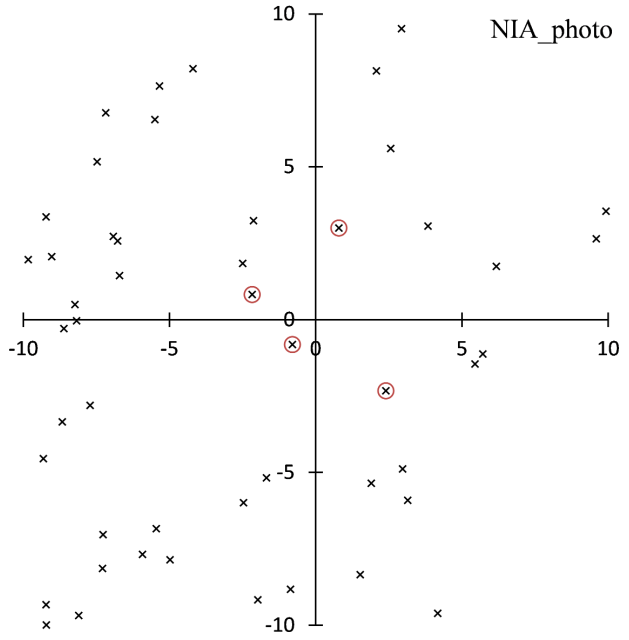

Figure 7a – Photographic meteors during the activity of the ι-Aquarids (northern branch) in the interval $124\overset{\circ}{.}7 < \lambda_s < 159\overset{\circ}{.}5$. The figure is centered at $(\lambda - \lambda_s, \beta) = (197\overset{\circ}{.}7, 3\overset{\circ}{.}9)$.

Table 7a – ι-Aquarids (northern branch) listed by Wright et al. (1957).

Code	λ_s	$\lambda - \lambda_s$	β	V_g	x	y	r	Note
H1-3429	124.7	196.9	6.9	30.4	0.8	3.0	3.1	
H3-3629	146.1	198.4	3.1	32.63	−0.8	−0.8	1.1	
H3-3663	149.0	199.8	4.7	28.53	−2.2	0.8	2.3	+
H3-3886	159.5	195.2	1.6	27.29	2.4	−2.3	3.3	STA
min	124.7	195.2	1.6	27.3				
max	159.5	199.8	6.9	32.6				
median	147.5	197.7	3.9	29.5				
mean	144.8	197.6	4.1	29.7				
sd	12.7	1.7	2.0	2.0				

Table 7b – Observations of ι-Aquarids (northern branch).

No.	α	δ	V_g	$\lambda - \lambda_s$	β	e	q	i	ω	Ω	λ_s	Stream
Wright et al.	330°52′	−4°57′									132.5	$\Delta\alpha + 62'$, $\Delta\delta + 9'$
LE-313	326.1	−3.4	39.0	208.8	9.7	0.940	0.100	28.9	328.8	118.3	118.3	Northern ι-Aquarids?
K1-91	321.7	−7.8	35.0	200.8	6.9	0.890	0.200	12.0	313.0	120.7	120.7	N ι-Aquariids
NI-61.7.11	326.9	−12.1	30.0	199.0	1.2	0.850	0.234	6.9	312.5	126.0	126.0	N.ι-Aquarids?
S2-50	352.5	−0.8	28.2	200.6	2.2	0.823	0.242	3.2	313.5	152.2	152.2	Northern ι-Aquarids
S3-159	350.1	0.6	26.1	198.1	4.4	0.777	0.302	5.2	307.4	153.1	153.1	Northern ι-Aquarids
LI-78	354.6	1.3	31.0	193.5	3.3	0.830	0.326	4.0	299.7	162.1	162.1	Northern ι-Aquarids

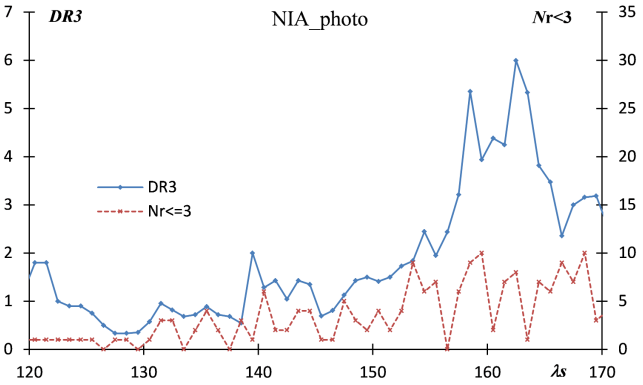

Figure 7b – The estimated activity profile of the ι-Aquarids (northern branch).

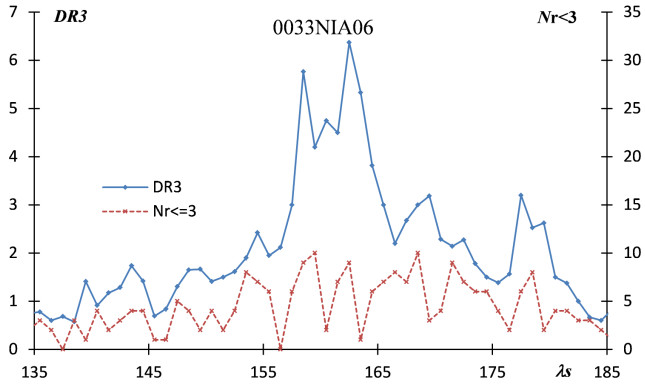

Figure 7d – The estimated activity profile of 0033NIA06 taking into account its estimated radiant shift.

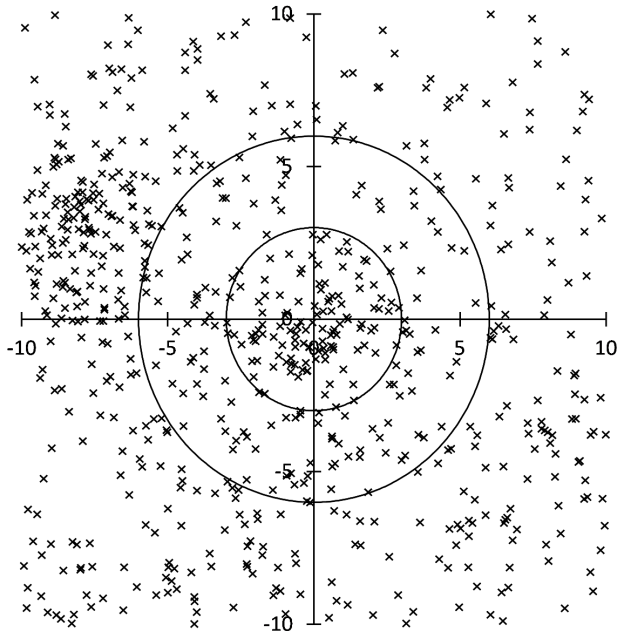

Figure 7c – Video meteor radiant distribution of 0033NIA06 ($151\overset{\circ}{.}3 < \lambda_s < 171\overset{\circ}{.}3$) taking into account its estimated radiant shift.

the northern branch would be late July to middle August. Some observers intended to identify such earlier meteor activity to the northern branch (Table 7b). It has been thought in that time, even now probably, that an ecliptic shower has northern and southern branches, ι-Aquarids and δ-Aquarids are the good examples. Many observers thought both ι-Aquarids and δ-Aquarids (with their branch together) are active around late July to early August naturally (Table 7b).

But we cannot confirm such early ι-Aquarids (northern branch) activity by video observations but the estimated profile indicates the increase of the activity to late August and early September (Figure 7b). We use the latest NIA observations in SD (0033NIA06) and get its radiant distribution taking its radiant shift into consideration (Figure 7c). The author will describe the details of the procedure in the paper announced in the Southern Arietids section.

This activity is confirmed by the activity profile by DR (Figure 7d) but this seems to be far from original ι-Aquarids (northern branch). Wright et al. (1957) gave the ephemeris for the northern branch till $\lambda_s = 157\overset{\circ}{.}5$ (B1950.0) and it is better to consider recent NIA observations are different from original ι-Aquarids (northern branch); 0033NIA02, 03 and 06 should be called (August) ω-Piscids as a new meteor shower.

3 Conclusions

We have been not free from the traditional conception of meteor showers; detected ones by photographic observations have been thought certain. Thousands of meteor orbits were enough to research meteor showers and many investigations revealed many "meteor showers". The Harvard surveys played an important role especially and many observers tried to catch their "meteor showers", that is, legendary ones. The IAUMDC (2018) meteor shower database (SD) succeeded to Harvard meteor shower list and is influenced by the legends.

This study shows such amount of photographic meteors is not enough to resolve minor shower activities. α-Virginids and ι-Aquarids (northern branch) are not AVB and NIA in SD. AVB and NIA of SD are conglomerate of false data with newly detected showers. ι-Aquarids (southern branch) and δ-Arietids are not recognized in recent video observations but their records should be kept in SD, because we could not reject the possibility that they were active in those days. Virginids are replaced by EVI but only one EVI meteor belongs to EVI; other "Virginids" seem to be sporadic. κ-Serpentids are not strictly equal to KSE; meteor activities in this area and period are so complex that large amount of video data is not enough to confirm details. The 18th position of SD should be kept for Southern Arietids; this is the secondary peak of STA complex. It is necessary to investigate minute structure of the STA complex; a large amount of video data has not been able to persuade researchers to the secondary core.

NDA is another misunderstanding of the legend; recent "NDA" should be called BPI properly. We need to find a regulation how to identify two observations concerning one meteor shower. Further, we suggest to find a preliminary designation for new detections before they obtain a permanent code once they are established.

References

Hoffmeister C. (1948). *Meteorströme*. J.A. Barth, Leipzig.

IAUMDC (2018). "IAU Meteor Data Center". `https://www.ta3.sk/IAUC22DB/MDC2007/` .

Jenniskens P. (2006). *Meteor Showers and their Parent Comets*. Cambridge University Press, Cambridge, UK.

Jenniskens P., Nénon Q., Albers J., Gural P. S., Haberman B., Holman D., Morales R., Grigsby B. J., Samuels D., and Johannink C. (2016). "The established meteor showers as observed by CAMS". *Icarus*, **266**, 331–354.

Koseki M. (2009). "Meteor shower records: A reference table of observations from previous centuries". *WGN, Journal of the IMO*, **37**, 139–160.

Koseki M. (2012). "Three components of 'Taurids'". *WGN, Journal of the IMO*, **40**, 129–138.

Koseki M. (2016). "Research on the IAU meteor shower database". *WGN, Journal of the IMO*, **44**, 151–169.

Koseki M. (2019a). "Showers of the IAU Meteor Data Center in the video data of SonotaCo: a simple and clear criterion for grading meteor showers". *WGN, Journal of the IMO*, **47**, 7–17.

Koseki M. (2019b). "Profiles of meteor shower activities inferred from the radiant density ratios (DR)". *WGN, Journal of the IMO*. (submitted).

McCrosky R. E. and Posen A. (1959). "New photographic meteor showers". *Astronomical Journal*, **64**, 25–27.

McCrosky R. E. and Posen A. (1961). "Orbital elements of photographic meteors". *Smithsonian Contributions to Astrophysics*, **4**, 15–84.

SonotaCo (2009). "A meteor shower catalog based on video observations in 2007-2008". *WGN, Journal of the IMO*, **37**, 55–62. (also `http://sonotaco.jp/doc/SNM/`).

Southworth R. B. and Hawkins G. S. (1963). "Statistics of meteor streams". *Smithsonian Contributions to Astrophysics*, **7**, 261–285.

Whipple F. L. (1940). "Photographic meteor studies. III. The Taurid shower". *Proceedings of the American Philosophical Society*, **83:5**, 711–745.

Whipple F. L. and Hawkins G. S. (1959). "Meteors". *Handbuch der Physik*, **52**, 519–564.

Wright F. W., Jacchia L. G., and Whipple F. L. (1957). "Photographic ι-Aquarid meteors and evidence for the northern δ Aquarids". *Astronomical Journal*, **62**, 225–233.

Handling Editor: Jürgen Rendtel

Fast thresholding options for video meteor imagery to obtain pixel exceedances

Peter S. Gural [1]

With the advent of high pixel count digital sensors and faster frame rates, the meteor image processing pipeline has needed to keep up with the increasing computational load. One can employ higher-end processors as well as implement more efficient image processing algorithms. One significant part of the pipeline is the detection process which often entails a thresholding operation. Various fast thresholding methods are examined herein and compared in their attributes, highlighting advantages and disadvantages in the application to video meteor detection.

Received 2019 October 27

1 Introduction

Both amateur and professional video meteor systems continue to evolve with the latest advances in sensor technologies. Meteor collection systems have been migrating towards multi-megapixel, progressive-scan digital sensors, and away from the traditional analog cameras with less than half-million pixels per frame. In particular the larger image sizes stress CPU processing loads when, for example, one uses a high-definition (HD) camera that has six times the pixel count of NTSC or PAL video. The computational issue has been partially offset by employing larger-capacity CPUs, but the increasingly larger pixel count restricts the ability to use multiple cameras feeding the same PC. In addition, the advent of innovative meteor collection systems requiring real-time responsiveness to meteor events has resulted in a re-examination of the entire image processing chain to increase computational efficiency while also improving detection and analysis robustness.

2 Image processing pipeline

The image processing pipeline for video meteor analysis consists of several components: capture of imagery, optional compression/storage of data, detection processing, astrometric and photometric calibration, optional confirmation or classification of true meteors, multi-site aggregation of tracks, trajectory estimation, and orbit calculation. In particular, the detection processing step often involves pre-conditioning of the imagery via dark subtraction, flattening, and hot-pixel removal, followed in many approaches by a thresholding operation to obtain pixel exceedances that rise above the background due to the passage of a meteor. The pipeline then employs a detection algorithm looking for a moving cluster of pixels or a propagating line segment across multiple frames. For example, a very fast clustering and tracking algorithm has been introduced (Gural, 2016) that dramatically improves runtime performance for meteor detection by a factor 40 over Hough transform methods.

To further complement work in fast detection, and as the primary focus of this paper, the upstream thresholding operation that feeds the clustering algorithm was re-examined in detail. The purpose was to explore options for making that particular processing component in the pipeline more efficient. This was driven by the design of a new instrument currently under development, a fireball-fragment tracking system. It is a system which requires minimal processing latency from the initial all-sky meteor detection, to steering a pan-tilt-zoom (PTZ) device onto a fireball target, for the purpose of obtaining high angular resolution images of the fragments.

3 Fast thresholding algorithms

To identify the fastest possible thresholding algorithm, various options were explored that are summarized in Table 1. A brief explanation of the column headings for the table is as follows:

- *Method* is a short descriptive title of the thresholding algorithm and reference ID number referred to in the text.
- *Tracking concept-of-operations or CONOPS* discriminates global from local methods of pixel level tracking for the background mean and noise standard deviation (σ). Very often, first-order response (FOR) filters with a fading memory coefficient α are used for tracking these statistics, with some methods using a "past" frame (P) that could be either the immediately previous frame or one that is further back in time. The basic form for a FOR filter for tracking the mean is shown in Equation 1. For faster computations on a PC, integer operations are often used and scaled up by a power-of-two to maintain significant digits in the filter update equation. Also using a power-of-two for the α coefficient allows for fast bit shifting rather than division when using integer operations:

$$\mu' = \mu + \frac{\mu - x}{\alpha}. \quad (1)$$

- The *mean (μ) and sigma (σ)* tracked background components require storage and memory fetches that can be time-consuming. When frame differencing is employed, the mean is often assumed to be approximately zero on average and often not tracked. For a global method, a single pair of mean and sigma values is applied to all pixels,

[1]Gural Software and Analysis LLC, 351 Samantha Drive, Sterling, Virginia USA 20164.
Email: pgural@gmail.com

IMO bibcode WGN-475-gural-thresholding
NASA-ADS bibcode 2019JIMO...47..151G

which thus assumes a uniform background characterization for the imagery. More typically, a "local" method is employed for obtaining the variable background statistics that are tracked on a per-pixel basis. This is to better handle background gradients and the higher variances for stars or hot pixels.

- The *thresholding* column shows the exceedance test operation applied to each pixel that uses some linear combination of the estimated background statistics for mean and sigma. In the past, "if" statements, which were necessary for most of the algorithms listed below, could break the CPU processor pipeline and slow down processing, depending on how the threshold test loop was implemented. Today, many CPUs run multiple paths to efficiently run through two branches of an if statement, and that has become less of an implementation concern.
- Some methods can get desensitized to future pixel exceedances based on the nature of the thresholding algorithm's latency or if a slow memory fade is used in the technique, which is indicated in the *desensitized threshold* column.
- *Latency* refers to the number of frames that must be processed before an initial frame-level detection process can be applied. Latency is an important consideration for real-time processing applications, but is less impactful in most meteor collection systems where a fixed offset delay can be tolerated during both processing the pixels and reporting a detection.
- The final column contains the timing results for a C implementation of each algorithm on an i7-4770 single core, presented in effective milliseconds per single frame processed. The image size used was standard HD of two megapixels (1920×1080 pixels), using a 2.1 sigma threshold or its equivalent, that results in 1.8% of pixels exceeding the threshold across the image. The C code module for each method is available upon request from the author.

A detailed description of the thresholding methods is as follows, with the item number below corresponding to the method ID in Table 1:

1. The fastest global method, using a past frame's global mean μ_G plus a user factor "k" times a global sigma σ_G as a threshold applied uniformly across the test frame's pixels. The best speed is achieved, since there are no extensive memory fetches for tracking or updating the background statistics. However, the method does assume that the imagery has a flat background, and note that stars/hot pixels will trigger threshold exceedances.

2. Global method that removes stationary features by differencing the current test frame relative to a past frame. Only the global sigma is computed from a previous computed difference, with the global mean assumed zero. The method handles background gradients across the field of view as well as star suppression, but assumes a flat variance across all the pixels, which can be inappropriate for star pixels whose variance can be proportional to the pixel intensity.

3. Global differencing method that employing a histogram binning approach for identifying pixel exceedances that avoids the `if` statement for thresholding each pixel. The highest difference value bins in the histogram are extracted until an exceedance percentage of the total image pixel count is reached. This method requires a linked list histogram counter to permit mapping the exceedance gray levels back to the actual row and column positions of the pixel exceedances.

4. One of the fastest local methods that makes two very simplifying assumptions, i.e., a past frame's image can be used as both the mean and variance estimate, such that the variance is assumed equal to the mean. The standard deviation for the threshold operation (square-root-of-two of the past image) is obtained through a fast table lookup indexed by the past image's integer gray value. A user-defined fixed sigma factor "k" is used to define a per pixel threshold to get a desired exceedance count. The method results in a background mean and sigma approximation that effectively varies across the image but represents a less than optimal mean and sigma estimate per pixel. However, it is as fast as the best global method and useful in very critical-runtime environments.

5. A fast method that is similar to method 4 but continuously tracks the background mean on a per pixel basis, using a FOR filter (fading memory) employing scaled integer operations and effectively folding in multiple earlier frames. The variance is assumed to be equal to the mean as in method 4, to avoid tracking it and minimize memory write and fetches, while the method has a more optimal mean estimation approach. The exceedance threshold level is controlled through the user-defined "k" factor. If the mean is updated using the current frame that contains a meteor, then the pixels associated with that meteor can get desensitized to future potential threshold crossers at those locations, at least until the tracking filter ramps back down to the mean level of those pixels. One can mitigate this by updating the mean for only those frames that the detection algorithm deems free of meteors.

6. Adjacent-in-time frame differencing, which suppresses the stationary stars and any background levels and gradients. The sigma values per pixel associated with the difference, is tracked with a FOR filter and the threshold is based on a zero mean with only a user-defined "k" factor times the per pixel sigma. Notice that the difference operation introduces both positive and negative values/streaks, which is often handled by taking

Table 1 – Thresholding algorithmic options and their characteristics.

ID	Method	Tracking CONOPS		Mean μ	Std Dev σ	Threshold operation	Desensitized threshold	latency # frames	2.1 σ ms
1	Global threshold	Past frame μ & σ		μ_{Global}	σ_{Global}	$T = \mu_{\text{G}} + k\sigma_{\text{G}}$	No	1	1.6
2	Global difference	Current − Past frame		≈ 0	σ_{Global}	$T = k\sigma_{\text{G}}$	No	1	2.7
3	Global histogram	Current − Past frame		No	No	% exceeds, no `if`s	No	1	3.1
4	Past for mean & σ	No tracking for mean & σ		P	$\sqrt{P}$	$T = P + k\sqrt{P}$	No	1	1.6
5	Mean, $\sqrt{\mu}$ for σ	Pixel μ	FOR $\alpha = 2^2$	μ	$\sqrt{\mu}$	$T = \mu + k\sqrt{\mu}$	Yes	1	1.9
6	2-Frame difference	Pixel σ	FOR $\alpha = 2^5$	≈ 0	σ	$T = k\sigma$	Minimal	2	2.6
7	MaxFilter	Maxpixel	FOR $\alpha = 2^Q$	No	No	FOR maxpixel	Yes	1	3.0
8	Past frame difference	Pixel σ	FOR $\alpha = 2^5$	≈ 0	σ	$T = k\sigma$	Minimal	1	4.1
9	Track mean & σ	Pixel μ & σ	FOR $\alpha = 2^5$	μ	σ	$T = \mu + k\sigma$	No	1	5.3
10	CAMS compression	Pixel level	N frames	μ	σ	Maxpixel, maxframe	Yes	N	8.9

the absolute value of the difference before thresholding. Because it requires a pair of frames, there is a latency of two frames before the threshold is calculated. Differencing also introduces a square-root-of-sigma increase in the noise background. The timing is quoted in the table as a per frame measurement despite requiring two frames to process, such that the method essentially distributes the computational load across two frame times. This was the underlying thresholding algorithm used by the MeteorScan video detection software (Gural, 2009).

7. MaxFilter is a new algorithmic innovation that involves no storage of mean or sigma. This method mimics the maximum-pixel-in-time approach of the CAMS compression technique (Gural, 2011; Jenniskens et al., 2011), but differs from the standard CAMS methodology by performing the exceedance test on a continuously running frame update. Thus, MaxFilter does not have the multi-frame latency of the standard CAMS compression (method 10) but does require spinning up the filter for a few hundred frames at start-up. Pixels are tested for values which are larger than the latest maximum-temporal-pixel "maxpixel" array entries. If larger, then the pixel is declared an exceedance, and the maxpixel array entry for that pixel is replaced with the new high pixel value. Then, all maxpixel values are updated applying a FOR filter on the latest image, whose α^{-1} coefficient is equal to a negative integer square power of "Q". The integer Q parameter actually controls the effective threshold sigma factor "k". For example, if $\alpha = 2^8$, such that $Q = -8$, the resultant sigma threshold factor is $k = 2.0$, as given by Equation 2:

$$k = -2.696e^{-5}Q^4 - 4.523e^{-4}Q^3 - 5.519Q^2 - 2.822e^{-1}Q, \quad (2)$$

valid for integer $Q = -2$ to -15 under white Gaussian noise.

Note that each pixel associated with an exceedance (values that were larger than the previous frame's maxpixel stored value for a given pixel), will now be desensitized to further threshold triggering until its maxpixel value ramps down at the rate given by the fading memory FOR coefficient α. For additional details, see the Appendix.

8. Similar to method 6 in terms of frame differencing, but is performed with a stride of one frame rather than stepping by frame pairs, thus nearly doubling the runtime cost. It is often used for differencing relative to a frame much further back in time, to catch an apparently slow-moving meteor that may dwell in the same pixel for several frames, and could thus get subtracted away with an adjacent-in-time frame difference. Meteors appearing in all-sky systems at low altitude angles, can experience this behavior given coarse camera angular resolutions. Thus, having a time gap of multiple frames when differencing is advisable in those situations.

9. The more classic background-tracking approach where a past frame that usually does not contain a meteor is used to update the mean and sigma per pixel with FOR filters using scaled integer arithmetic for fast processing. A user-defined fixed sigma factor "k" is used to set a per-pixel threshold that yields a desired exceedance count and the threshold may optionally include an extra bias term (Vida, 2019, Personal communication on the threshold algorithm used by the GMN systems). The runtime costs are higher than other methods due to the extra memory fetches and writes for each pixel's mean, sigma, and threshold test, as well as the associated update operations for those statistical tracking arrays.

10. The CAMS compression approach to pixel threshold exceedance identification. This method requires a tolerance to long multi-frame latency, to provide time to form the four arrays of mean, sigma, maximum temporal pixel (called maxpixel), and the frame numbers of the maxpixel pixels (called maxframe). The fixed number of frames N_{f} making up a compression block, which is used to form these four image arrays, governs the equivalent threshold sigma factor (for example, $2.1\sigma = 56$ frames in the block). To identify the exceedance pixels for a specific frame number in the imagery block that is undergoing threshold testing, one locates the maxframe array elements that possess the same frame number as the frame number under test. Thus, a very fast exceedance pixel extraction is achievable based solely on array indexing and no if statements after the compression array formation (Gural, 2016). For this method,

the runtime quote of the last column in Table 1 actually includes the time to form the four arrays averaged over the total frame count of the compression block. The bulk of the processing load is in the compression step over the block of frames, which once done, the pixel exceedance retrieval is extremely fast. The relationships between the threshold sigma scaling factor and frame count in the compression block for white Gaussian noise are given in Equations 3–5, as follows:

$$k = +0.009591m^5 - 0.1248m^4 + 0.6479m^3 - 1.762m^2 + 3.357m - 0.8418; \quad (3)$$

$$m = \log_{10} N_f; \quad (4)$$

$$N_\mathrm{f} = 10^{0.1864k^2+0.2899k+0.3211}. \quad (5)$$

In the course of this study, a formula was obtained that relates the desired percentage of pixels "$P\%$" from an image threshold operation to the k sigma factor, i.e., the number of pixels that exceed a mean plus k times sigma threshold has the relationship shown in Equation 6 given $r = \log_{10} P\%$ and the noise being Gaussian-distributed:

$$k = 2.3206 - 0.8612r - 0.1036r^2 - 0.03171r^3 - 0.0253r^4 - 0.01012r^5 - 0.001335r^6. \quad (6)$$

Once a threshold is applied to a new frame and an exceedance list of pixel positions is obtained, the highlighted pixel positions and intensities are usually fed to a detection module that looks for linearly propagating line segments across frames. Blob and cluster detectors, small kernel matching methods, and Hough transforms are example detection algorithms that have been implemented in various meteor applications (Gural, 2016; Molau & Gural, 2005; Gural, 2009). The most efficient and robust meteor processing pipeline for a given application will likely use some thresholding option, although the choices indicated herein may not be totally exhaustive. Only the most efficient in processing time that the author was aware of, plus those in common use, have been addressed. Other ideas for fast thresholding approaches are welcomed by the author.

References

Gural P. S. (2009). "METEORSCAN – Documentation and User's Guide Version 2.2". `ftp://aquarid.physics.uwo.ca/pub/gural/MeteorScan300/METEORSCAN.doc` .

Gural P. S. (2011). "The California All-Sky Meteor surveillance (CAMS) system". In Asher D. J., Christou A. A., Atreya P., and Barentsen G., editors, *Proceedings of the International Meteor Conference, Armagh, Northern Ireland, 16–19 September 2010*. IMO, pages 28–31.

Gural P. S. (2016). "A fast meteor detection algorithm". In Roggemans A. and Roggemans P., editors, *Proceedings of the International Meteor Conference, Egmond, the Netherlands, 2–5 June, 2016*. IMO, pages 96–104.

Jenniskens P., Gural P. S., Dynneson L., Grigsby B. J., Newman K. E., Borden M., Koop M., and Holman D. (2011). "CAMS: Cameras for Allsky Meteor Surveillance to establish minor meteor showers". *Icarus*, **216**, 40–61.

Molau S. and Gural P. S. (2005). "A review of video meteor detection and analysis software". *WGN, Journal of the IMO*, **33**, 15–20.

Handling Editor: Marc Gyssens

Appendix

Some additional details of the MaxFilter algorithm are provided in this Appendix. The method tries to minimize the computer memory storage and retrieval requirements, as well as mimic the maxpixel properties of the CAMS compression algorithm. But unlike the latter, MaxFilter operates on a frame-by-frame basis with no multi-frame latency, thus the algorithm identifies exceedances and updates the maxpixel array in a continuous fashion as the frames are read in. Its downside is that a mean and standard deviation are not tracked, although the running maxpixel can be considered a high biased version of the mean.

The MaxFilter algorithm is described within the item devoted to method 7, above. The result of the process over time is that recent high-value (exceedance) pixels in the maxpixel array slowly ramp back down to approach the mean before getting triggered again as an exceedance pixel. This is visualized in Figure 1, which shows a single maxpixel array element as a function of frame number that has undergone several threshold jumps in a white Gaussian noise environment. Curiously, it is the FOR fading-memory coefficient α that actually governs the effective k sigma factor. Note that Equation 2 is given for integer values of Q, which results in k steps of approximately 0.25σ. A finer stepping resolution in the sigma factor is possible, but involves more computational loading, since α is no longer a power-of-two with its associated fast bit shift operations.

The method requires an initialization for the MaxFilter maxpixel array elements, which can be either the first image ingested, or a CAMS compressed block of N_f frames that yields the CAMS maxpixel array on output. Either way, several frames of input are required to spin up the maxpixel array before a good threshold exceedance list can start to be processed for detections. The number of frames required for N_f is given by Equation 5.

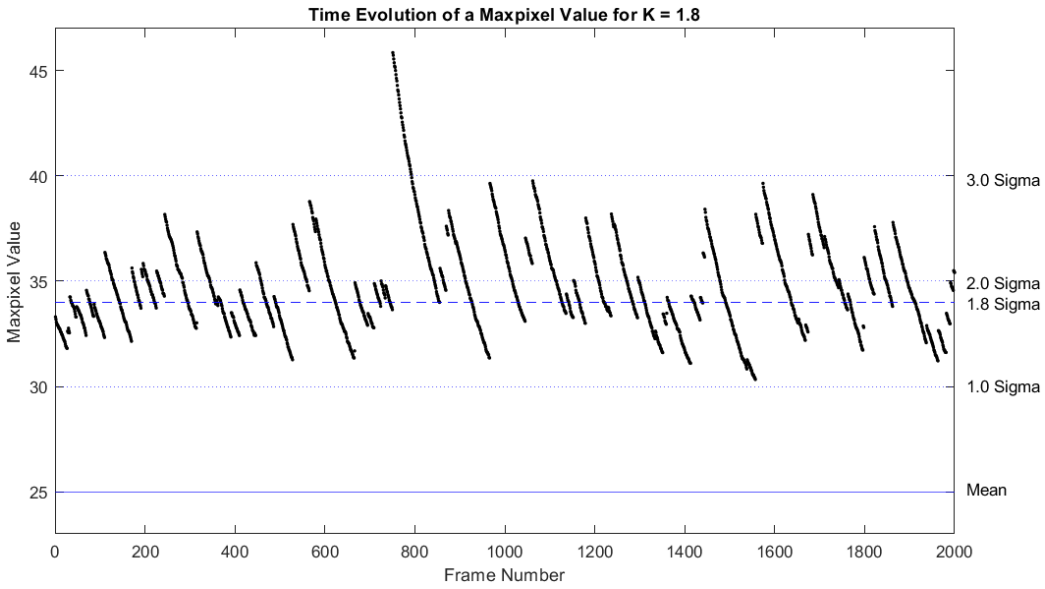

Figure 1 – The MaxFilter temporal evolution of a maxpixel value where each jump up is a threshold exceedance trigger event for $k = 1.8$ (corresponding to $Q = -7$). The simulated frame sequence consisted of a background mean of 25 plus sigma, with sigma equal to 5 for white Gaussian noise.

The December ρ Virginids and Comet C/1961 T1 (Seki)

John Greaves [1]

An old analysis of Dutch Meteor Society video meteor orbits is revisited in the light of modern much larger meteor orbit databases and assessed against the IAU Meteor Data Center's shower listings using D criterion testing. Eleven orbits are matched directly whilst forty five are found if a perihelion adjustment is applied. The similarity to the December ρ Virginids is noted.

Received 2019 June 5

1 Introduction

In Greaves (2000), and references therein, the similarity between three Dutch Meteor Society video meteor orbits and that of the comet C/1961 T1 (Seki), 1961 VIII old style (e.g. Marsden & Roemer, 1978), is outlined. The result from that small list of orbits gleaned from a pioneering and way ahead of its time two station survey has been reassessed, as in recent years an increasing numbers of two to multi-station meteor orbits have become publicly available. The resulting objects are matched against the IAU Meteor Data Center (MDC), (e.g. Jopek & Kanuchova, 2017[a], in order to assess if any of the new meteor showers from published multi-station video meteor orbits listed there are a match or whether the potential shower is distinct.

Orbits from the publicly available datasets at SonotaCo[b] and EDMOND, (e.g. Kornos et al., 2014), are matched against the same basic orbit for C/1961 T1 used in Greaves (2000) (e.g. Marsden & Roemer, 1978) by utilising the Jopek (1993) modification of the Southworth & Hawkins (1963) D criterion.

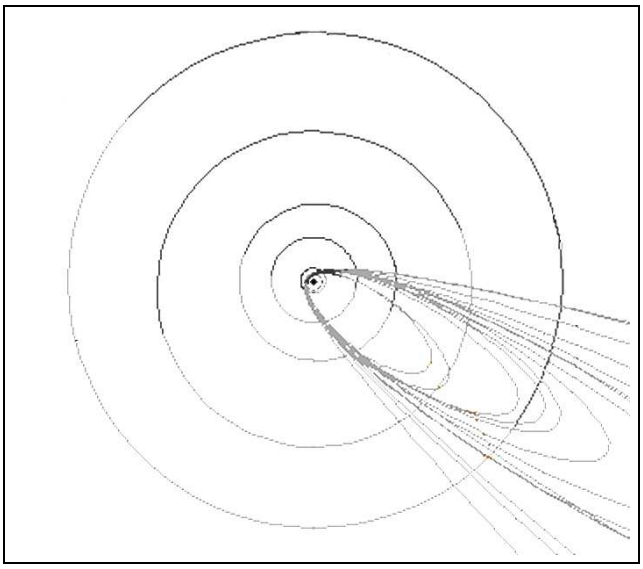

Figure 1 – The eleven derived meteor orbits plus two IAU MDC listed formal orbits for the DRV shower as viewed from the North Ecliptic Pole, outermost planetary orbit shown is that of Neptune.

2 Results

Eleven meteor orbits from the above datasets are matched against the comet's basic orbit. Examination of the orbits, solar longitudes and radiants held at the IAU MDC suggest a close relationship to the December ρ Virginids, IAU MDC code DRV number 502, first mentioned in Rudawska & Jenniskens (2014) as well as the aforementioned Kornos et al. (2014) which is an adjacently placed article appearing in the same publication. Indeed, the three orbits matched from the EDMOND database are already logged as connected to the DRV shower by the EDMOND dataset.

The two most extreme of the derived shower orbits in the IAU MDC database are taken, with the largest and smallest values in perihelion and ascending node respectively used, taking Kornos et al. (2014) for the smaller values and Jenniskens et al. (2018) for the larger ones. These plus the eleven derived orbits and the orbit used for C/1961 T1 (Seki) are plotted to highlight their similarity. Figure 1 depicts a representation as viewed from the Ecliptic North Pole and Figure 2 is the same but viewed looking into the Ecliptic Plane.

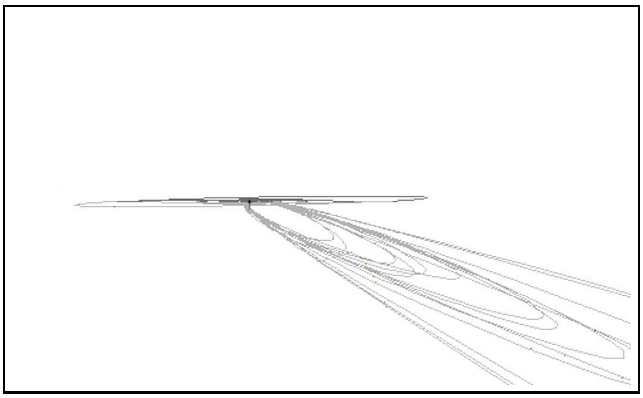

Figure 2 – The eleven derived meteor orbits plus two IAU MDC listed formal orbits for the DRV shower as viewed from the Ecliptic Plane, dark grey sections of the orbits are above the plane, light grey below.

Throughout there is some slight offset in Solar Longitude and radiant position between these meteors and the same values listed in the IAU MDC entries for the December ρ Virginids. However these are only on the order of a few degrees, with the values from different authors listed at the IAU MDC differing from each other to a similar level.

[1]Northants, UK. Email: cpmjg@tutanota.com

IMO bibcode WGN-475-greaves-sekiids
NASA-ADS bibcode 2019JIMO...47..156G

[a]mirrored at
http://pallas.astro.amu.edu.pl/~jopek/MDC2007/index.php

[b]http://sonotaco.jp/doc/SMN

Table 1 – The used identifier (EDMOND data ending in 'ED'), perihelion distance q in Astronomical Units, eccentricity e, inclination *incl*, argument of perihelion *argper*, ascending node *ascnode* and derived D criterion related to the comet orbit results from the analysis. DRV1 gives the orbital elements from Kornos et al. (2014) and DRV2 those from Jenniskens et al. (2018). The orbital elements used for C/1961 T1 (Seki) (e.g. Marsden & Roemer, 1978) are also given.

Local Time Identifier	q	e	*incl*	*argper*	*ascnode*	D
20071201_022250	0.772	0.951	155.9	123.7	248.0	0.10
20091202_042903	0.798	1.025	153.9	128.6	249.6	0.09
20101202_023002	0.784	1.042	154.7	126.7	249.3	0.09
20121129_043054	0.762	0.977	156.7	122.6	246.8	0.08
20131203_014059ED	0.803	0.974	155.0	128.6	250.9	0.09
20141202_045359	0.791	0.964	157.8	126.6	249.3	0.09
20141203_044213ED	0.798	0.957	154.7	127.6	250.7	0.10
20151202_045212	0.782	0.980	155.2	125.6	249.1	0.08
20161130_032001ED	0.781	0.956	153.5	125.1	248.1	0.09
20161203_054016	0.800	0.983	153.1	128.2	250.9	0.10
20171121_042729	0.720	1.010	153.0	117.4	238.4	0.09
DRV1	0.776	0.920	154.8	123.8	253.2	
DRV2	0.796	0.930	151.0	127.0	258.4	
C/1961 T1 (Seki)	0.681	0.992	155.7	126.6	247.4	

Table 1 provides the orbital elements used for the comet, the two DRV representative orbits from the IAU MDC and the individual matched orbits from the SonotaCo and EDMOND datasets, both tagged using their local time identifications with the EDMOND orbits ending with 'ED' in order to distinguish them.

3 Discussion

Neslusan et al. (1998) note that there are comets with associated streams having orbits that do not bring them sufficiently close to the Earth's orbit in order for such streams to actually exist without some evolution of the meteoroid stream. The paper then goes on to list methods that allow for detection of these adjusted streams based on possible changes in their orbit, applying them to both the pre- and post- perihelic arc cases. The paper also presents a DOS executable file (MetRad, sadly no longer available online as far as the author can ascertain) that takes the orbital elements of comets as input and presents the predicted circumstances of any potential shower along with an assessment of its reality via the Southworth & Hawkins (1963) D criterion. The program also generates the modified orbital elements from this result.

Accordingly the orbit for C/1961 T1 (Seki) listed in Table 1 is transformed and the various results assessed. The pre-perihelic arc presents no viable candidate but the post-perihelic arc presents several around a borderline of 0.088 to 0.107 in value for the D criterion. There was little difference in resulting radiant position and Solar Longitude value amongst these methods with some giving exactly the same as another.

For examination purposes the 'Q' or '*Adjustment of the orbit by variation of the perihelion distance – the q-adjustment*' due to the (Hasegawa, 1990) method is used. The elements for this orbit are presented in Table 2 followed by a 'Q' to distinguish them.

This resulted in matching forty five meteor orbits from a combined dataset of orbits derived from SonotaCo and EDMOND, with roughly two thirds of the results from SonotaCo and one third from EDMOND. Rather pleasantly one of the Dutch Meteor Society video meteor orbit candidates from the original paper is also recovered, DMS V95746. Why the other two are not recovered is not clear. This suggests that the December ρ Virginids are derived from C/1961 T1 (Seki) with the stream having undergone some slight evolution in at least perihelion distance that has made them Earth crossing.

4 Conclusion

D criterion assessment using SonotaCo and EDMOND multistation meteor orbits suggests that a sparse number of meteor orbits can be associated with C/1961 T1 (Seki) thus helping confirm an intimation from two decades ago based on a pioneering observing campaign that provided a much, much smaller data sample. Published methods for the modification of cometary orbits to reflect the potential evolution of meteoroid streams can also increase the likely number of candidates and present a means by which comet to meteor associations can be extended, at least for higher inclined orbits and ones that have not been too modified away from their original orbit by Jovian perturbations.

Acknowledgements

DMS, SonotaCo and EDMOND are strongly thanked for making their data publicly accessible as soon as possible without which analyses are of course completely impossible.

References

Greaves J. (2000). "The Sekiids". *Radiant*, **22:3**, 41–44.

Hasegawa I. (1990). "Predictions of the meteor radiant point associated with a comet". *PASJ*, **42**, 175–186.

Jenniskens P., Baggaley J., Crumpton I., Aldous P., Pokorny P., Janches D., Gural P. S., Samuels D.,

Table 2 – The used identifier (EDMOND data ending in 'ED'), perihelion distance q in Astronomical Units, eccentricity e, inclination *incl*, argument of perihelion *argper*, ascending node *ascnode* and derived D criterion related to the post-perihelion arc perihelion adjusted comet orbit results from the analysis. DRV1 gives the orbital elements from Kornos et al. (2014) and DRV2 those from Jenniskens et al. (2018). The orbital elements derived for the C/1961 T1 (Seki) (e.g. Marsden & Roemer, 1978) post-perihelion arc perihelion adjusted orbit (Hasegawa, 1990) as generated using MetRad (Neslusan et al., 1998) are also given.

Local Time Identifier	q	e	*incl*	*argper*	*ascnode*	D
DMSV95746	0.752	0.944	158.3	120.5	239.4	0.09
20071201_022250	0.772	0.951	155.9	123.7	248.0	0.07
20071202_040535	0.788	1.067	156.8	127.6	249.1	0.08
20071205_034437	0.794	1.017	154.2	127.9	252.1	0.07
20071206_034445	0.797	0.969	153.5	127.7	253.1	0.09
20081206_045120	0.847	0.963	158.2	135.6	253.9	0.09
20091127_024224	0.762	0.919	153.7	121.7	244.5	0.09
20091202_042903	0.798	1.025	153.9	128.6	249.6	0.05
20091206_032356	0.805	1.009	153.5	129.5	253.6	0.08
20091206_044235ED	0.817	1.009	152.8	131.3	254.1	0.08
20091206_045952	0.814	1.000	154.5	130.6	253.7	0.06
20091206_052950	0.852	0.966	154.2	136.4	253.7	0.10
20101202_023002	0.784	1.042	154.7	126.7	249.3	0.06
20101202_045154	0.766	0.989	155.5	123.5	249.4	0.09
20101205_051808	0.794	0.996	159.6	127.6	252.4	0.10
20111124_051733	0.758	1.012	159.8	122.5	241.0	0.09
20111125_041820	0.773	1.015	159.4	124.7	242.0	0.09
20111204_050523	0.779	0.982	156.0	125.2	251.1	0.09
20111205_031845	0.795	1.021	153.6	128.1	252.1	0.08
20121128_030513ED	0.803	0.941	158.4	128.0	246.1	0.08
20121129_043054	0.762	0.977	156.7	122.6	246.8	0.07
20121205_025612	0.792	1.040	156.4	128.0	252.8	0.09
20121205_045436	0.798	1.031	152.5	128.7	252.9	0.10
20131130_031015ED	0.761	0.947	155.3	122.0	247.9	0.10
20131203_014059ED	0.803	0.974	155.0	128.6	250.9	0.04
20131203_040604	0.772	1.023	157.7	124.8	250.6	0.10
20131204_010016ED	0.789	0.945	155.2	126.1	251.8	0.10
20131204_035400ED	0.800	0.931	155.8	127.6	252.0	0.09
20131205_052857	0.813	0.961	160.0	130.0	252.7	0.09
20141202_045359	0.791	0.964	157.8	126.6	249.3	0.06
20141203_044213ED	0.798	0.957	154.7	127.6	250.7	0.06
20151202_035615ED	0.768	0.995	153.1	123.9	249.4	0.09
20151202_045212	0.782	0.980	155.2	125.6	249.1	0.05
20151206_034159ED	0.845	1.037	156.4	136.0	253.5	0.10
20151208_061642ED	0.825	0.953	155.8	131.9	255.5	0.08
20161130_032001ED	0.781	0.956	153.5	125.1	248.1	0.06
20161203_054016	0.800	0.983	153.1	128.2	250.9	0.06
20161204_034947ED	0.829	0.998	157.6	133.0	252.2	0.06
20161205_045231ED	0.814	1.042	154.6	131.2	253.3	0.07
20171121_042729	0.720	1.010	153.0	117.4	238.4	0.10
20171122_032609	0.753	1.017	158.8	122.0	239.4	0.10
20171129_051323	0.778	1.073	157.5	126.3	246.6	0.09
20171205_041018	0.807	1.052	155.6	130.3	252.6	0.07
20171205_051514	0.806	0.962	151.4	128.9	252.6	0.10
20171206_030012	0.797	1.019	154.8	128.3	253.6	0.09
DRV1	0.776	0.920	154.8	123.8	253.2	
DRV2	0.796	0.930	151.0	127.0	258.4	
C/1961 T1 (Seki)	0.788	0.992	155.7	126.6	247.4	

Albers J., Howell A., Johannink C., Breukers M., Odeh M., Moskovitz N., Collison J., and Ganju S. (2018). "A survey of southern hemisphere meteor showers". *Planetary and Space Science*, **154**, 21–29.

Jopek T. J. (1993). "Remarks on the meteor orbital similarity D-criterion". *Icarus*, **106**, 603–607.

Jopek T. J. and Kaňuchová Z. (2017). "IAU Meteor Data Center-the shower database: A status report". *Planetary and Space Science*, **143**, 3–6.

Kornoš L., Matlovič P., Rudawska R., Tóth J., Hajduková, M. J., Koukal J., and Piffl R. (2014). "Confirmation and characterization of IAU temporary meteor showers in EDMOND database". In Jopek T. J., Rietmeijer F. J. M., Watanabe J., and Williams I. P., editors, *The Meteoroids 2013, Proceedings of the Astronomical Conference held at A.M. University, Poznań, Poland, Aug. 26-30, 2013*. A.M. University Press, pages 225–233.

Marsden B. G. and Roemer E. (1978). "Comets in 1975". *Royal Astronomical Society, Quarterly Journal*, **19**, 59–89.

Neslusan L., Svoren J., and Porubcan V. (1998). "A computer program for calculation of a theoretical meteor-stream radiant". *Astronomy and Astrophysics*, **331**, 411–413.

Rudawska R. and Jenniskens P. (2014). "New meteor showers identifed in the CAMS and SonotaCo meteoroid orbit surveys". In Jopek T. J., Rietmeijer F. J. M., Watanabe J., and Williams I. P., editors, *The Meteoroids 2013, Proceedings of the Astronomical Conference held at A.M. University, Poznań, Poland, Aug. 26-30, 2013*. A.M. University Press, pages 217–224.

Southworth R. B. and S. H. G. (1963). "Statistics of meteor streams". *Smithsonian Contributions in Astrophysics*, **7**, 261–285.

Handling Editor: Javor Kac

Preliminary results

Results of the IMO Video Meteor Network — September 2018

Sirko Molau[1], *Stefano Crivello, Rui Goncalves, Carlos Saraiva, Enrico Stomeo, Jörg Strunk, Javor Kac*

During 2018 September, 84 cameras of the IMO Video Meteor Network recorded nearly 55 000 meteors during more than 14 400 hours of observing time. MeteorFlux tool has been upgraded to present results generated using three data sets: real-time data, temporary data set, and final data set. The flux density profiles of the α-Aurigids and the September ε-Perseids are presented and both show similar activity profiles in 2018 when compared to the average profile of the previous years. The population index profile of the September ε-Perseids is also presented.

Received 2019 November 6

1 Introduction

The unusually pleasant weather of the previous month continued in September 2018. At the beginning of the month and on September 22 the conditions were variable, but at all other times almost every camera could obtain long series of observing nights. Highlight was September 16/17, when 80 of 84 cameras were in operation.

71 cameras managed to obtain observation during twenty or more observing nights, and seven cameras (mostly in Portugal and Italy) could observe without any break at all. These are clearly record-breaking results in the twenty-years history of the IMO Network.

Since nights are getting longer in September, this results inevitably in an all-time high of 14 400 hours of effective observing time (Table 1 and Figure 1) – 150 hours more than in the previously best month September 2016 (Molau et al., 2017). However, the average rate of 3.8 meteors per hour was lower than in previous years and, consequently, those nearly 55 000 meteors we recorded are only the second-best September output ever.

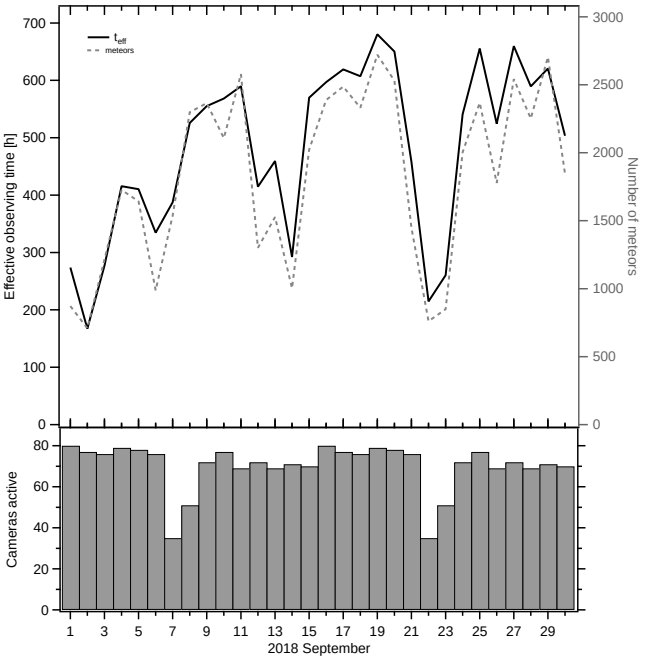

Figure 1 – Monthly summary for the effective observing time (solid black line), number of meteors (dashed gray line) and number of cameras active (bars) in 2018 September.

2 MeteorFlux

Unfortunately, we have a significant backlog in analyzing IMO Network video data. Until now, interested researchers and observers have had to wait for a long time until our flux density data became available. That has changed with the new version of MeteorFlux, which went live in September 2019. Since there have been no changes to the software in the past six years, Sirko familiarized himself step-by-step with the source code and implemented long-awaited features himself. Among others, two new data upload channels have been implemented (Figure 2).

The previous workflow was as follows: Data from a video camera was recorded and analyzed by MetRec. The camera operator checked and improved the data set with PostProc in the following days or weeks (by deleting false detections, for example), before uploading it by `ftp` to a central fileserver. IMO Network administrators would check the data with PostProc once more, before it was manually ingested into the MeteorFlux database. Thanks to the four-eyes-principle, this data will have the best possible quality, but there is also a significant delay in publication of currently more than a year.

Now there is the alternative option that allows the camera operator to upload the data after their check check directly into a *temporary* MeteorFlux database. Hence, the timeliness is improving dramatically and the quality is getting only a little worse, because it is only the double-check by a second person that is skipped. Data will be kept in the temporary database until the finally checked data of the corresponding month are uploaded. The MeteorFlux graphical user interface at `https://meteorflux.org` remains unchanged – analysts only have to select whether they want to work on the temporary or final database.

[1]Abenstalstr. 13b, 84072 Seysdorf, Germany.
Email: `sirko@molau.de`

IMO bibcode WGN-475-molau-vidsep
NASA-ADS bibcode 2019JIMO...47..160M

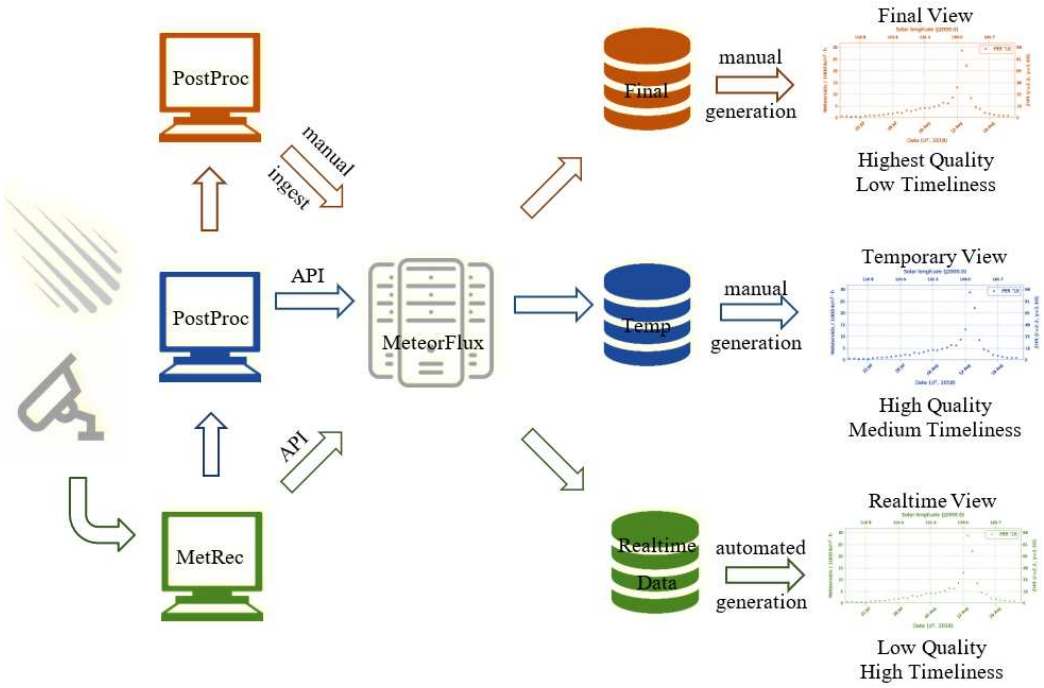

Figure 2 – Since September 2019, MeteorFlux is offering three different upload channels for video data.

Extending this idea through to its logical endpoint, a third upload channel was implemented. Here, MetRec is uploading data directly during the observation to the MeteorFlux server. These data are naturally error-prone, because they still contain all the false detections. This effect is mitigated by the fact that false detections are typically sporadic and not shower meteors. In addition, there is a specific routine that filters out questionable data automatically. Based on the real-time database, MeteorFlux is automatically generating every five minutes for every active meteor shower an activity profile of the past few days until now. The real-time display at `https://meteorflux.org/rt` is not suitable for further shower analyses, but it presents interested observers with the activity level of the currently active showers and indicates whether there is any kind of unusual activity ongoing. The interface is designed such that real-time activity profiles can be easily integrated into other websites. Since October 2018, for example, they have been displayed on the IMO homepage.

The following analyses of two meteor showers rely on the *final* data set of September 2018. However, at the time of writing of this report, almost half of the September 2019 data are already available in the temporary database.

3 α-Aurigids

The α-Aurigids at the borderline of August to September show in the long-term profile of 2011–2017 an almost constant activity level with just a small increase in rates between 155° and 163° solar longitude. The 2018 activity profile matches roughly to the average profile with the activity between 158° and 161° solar longitude slightly above the background level (Figure 3).

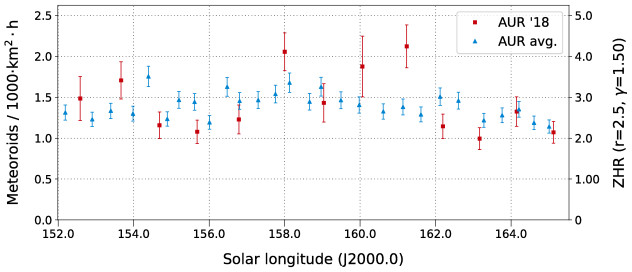

Figure 3 – Flux density profile of the α-Aurigids 2018 (darker/red) and the average of 2011–2017 (lighter/blue), derived from video data of the IMO Network.

4 September ε-Perseids

The long-term profile of the September ϵ-Perseids 2011–2017 (without 2013, when the shower experienced a significant outburst) is more interesting. It shows a continuous increase in rates from 163.°0 to 165.°5 solar longitude, thereafter declining rates until 166.°0

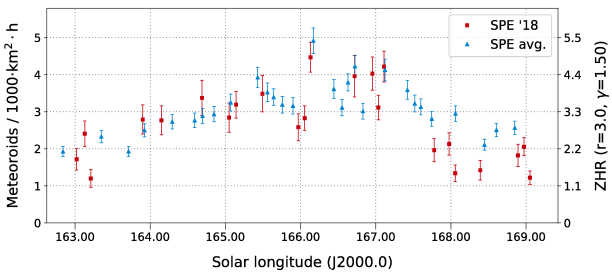

Figure 4 – Flux density profile of the September ε-Perseids 2018 (darker/red) and in the average of 2011–2017 (without 2013, lighter/blue), derived from video data of the IMO Network.

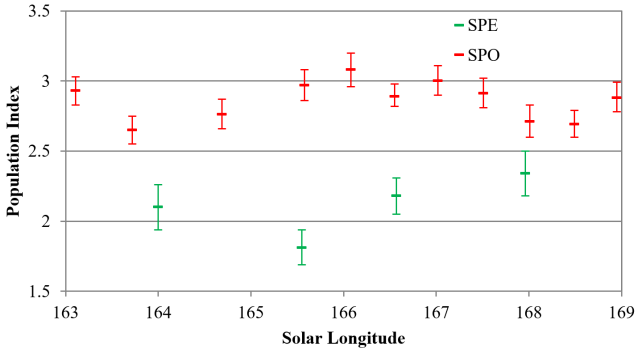

Figure 5 – Population index of the September ε-Perseids and sporadic meteors in September 2018.

solar longitude, and finally another increase until the real peak at 167.°0 solar longitude. Thereafter rates decline and reach the background level at 169.°0 solar longitude. 2018 data follow this activity pattern quite well (Figure 4).

Of particular interest is a single outlier at 166.°2 solar longitude, which is visible in the long-term profile and in the 2018 data, and which is stronger than the main peak. Chance or real structure? Looking at the live graph of the IMO VMDB data from the September ε-Perseids 2018 (International Meteor Organization, 2018) we also see a double peak at 167.°2 and 168.°2, but the visual data set and therefore also the temporal resolution is much smaller.

The population index of the September ε-Perseids (Figure 5) shows close to the peak significantly smaller values than the sporadic meteors. Towards the start and end of the activity interval, when the "sporadic pollution" is increasing, the values are approaching each other.

References

International Meteor Organization (2018). "September ε-Perseids 2018 campaign Live Graph". `http://www.imo.net/members/imo_live_shower/summary?shower=SPE&year=2018` .

Molau S., Crivello S., Goncalves R., Saraiva C., Stomeo E., and Kac J. (2017). "Results of the IMO Video Meteor Network – September 2016". *WGN, Journal of the IMO*, **45:1**, 18–23.

Handling Editor: Javor Kac

Code	Name	Location	Camera	FOV [°²]	Stellar LM [mag]	Eff.CA [km²]	Nights	Time [h]	Meteors
ARLRA	Arlt	Ludwigsfelde/DE	Ludwig2 (0.8/8)	1483	6.2	3812	27	167.5	964
BERER	Berkó	Ludányhalászi/HU	Hulud1 (0.8/3.8)	5524	4.8	3829	16	133.4	649
BIATO	Bianchi	Mt. San Lorenzo/IT	Omsl1 (1.2/4)	6422	4.0	1699	28	184.2	600
BOMMA	Bombardini	Faenza/IT	Mario (1.2/4.0)	5779	3.3	644	29	238.2	1162
BREMA	Breukers	Hengelo/NL	Mbb3 (0.75/6)	2399	4.2	641	24	174.5	353
BRIBE	Klemt	Herne/DE	Hermine (0.8/6)	2369	4.2	674	25	167.3	698
		Bergisch Gladbach/DE	Klemoi (0.8/6)	2374	4.6	1123	29	194.6	739
CARMA	Carli	Monte Baldo/IT	Bmh2 (1.5/4.5)*	4243	3.0	371	27	121.7	1304
CASFL	Castellani	Monte Baldo/IT	Bmh1 (0.8/6)	2402	5.0	1633	26	200.2	598
CINFR	Cineglosso	Faenza/IT	Jenni (1.2/4)	5995	3.9	1240	29	250.3	1084
CRIST	Crivello	Valbrevenna/IT	Arci (0.8/3.8)	5566	4.6	2571	30	229.6	824
			Bilbo (0.8/3.8)	5441	4.2	1764	30	224.9	1103
			C3P8 (0.8/3.8)	5489	4.2	1603	30	206.3	757
			Stg38 (0.8/3.8)	5574	4.4	1905	29	137.1	956
ELTMA	Eltri	Venezia/IT	Met38 (0.8/3.8)	5607	4.3	2381	27	186.0	642
FORKE	Förster	Carlsfeld/DE	Akm3 (0.75/6)	2387	5.1	2145	22	152.5	725
GONRU	Goncalves	Foz do Arelho/PT	Farelho1 (0.75/4.5)	2260	3.0	206	13	80.6	35
		Tomar/PT	Templar1 (0.8/6)	2212	5.3	1873	30	265.7	1049
			Templar2 (0.8/6)	2341	5.0	1718	30	267.1	755
			Templar3 (0.8/8)	1438	4.3	542	29	243.9	373
			Templar4 (0.8/3.8)	5180	3.0	497	30	264.2	754
			Templar5 (0.75/6)	2309	5.0	2248	28	224.8	672
GOVMI	Govedič	Središče ob Dravi/SI	Orion2 (0.8/8)	1471	5.5	2170	26	188.8	622
			Orion3 (0.95/5)	3152	4.9	2130	25	201.0	313
			Orion4 (0.95/5)	3818	4.3	1634	26	189.7	274
HERCA	Hergenrother	Tucson/US	Salsa3 (0.8/3.8)	2336	4.1	538	23	198.8	552
HINWO	Hinz	Schwarzenberg/DE	Hinwo1 (0.75/6)	2375	5.1	1889	25	178.6	649
IGAAN	Igaz	Budapest/HU	Hupol (1.2/4)	2414	3.6	409	14	97.3	106
JONKA	Jonas	Budapest/HU	Husor (0.95/4)	3988	3.6	729	25	201.6	298
			Husor2 (0.95/3.5)	2468	3.9	716	27	155.7	363
KACJA	Kac	Kamnik/SI	Cvetka (0.8/3.8)*	5334	4.3	2028	21	123.4	678
			Rezika (0.8/6)	2269	4.4	863	21	128.3	792
			Stefka (0.8/3.8)	5458	3.6	911	19	121.2	418
		Kostanjevec/SI	Metka (0.8/12)*	711	6.4	2133	17	84.8	244
		Ljubljana/SI	Sraka (0.8/6)	2348	4.8	1595	26	150.7	607
KOSDE	Koschny	La Palma/ES	Icc9 (0.85/25)*	660	6.7	2835	28	179.5	2133
			Lic2 (3.2/50)*	1933	6.5	6554	26	133.3	1472
LOJTO	Łojek	Grabniak/PL	Pav57 (1.0/5)	728	6.2	2087	13	112.7	507
MACMA	Maciejewski	Chełm/PL	Pav35 (0.8/3.8)	5329	4.0	1530	22	131.3	459
			Pav36 (0.8/3.8)*	5484	4.0	1501	22	171.6	696
			Pav43 (0.75/4.5)*	2251	4.7	1484	23	175.4	640
			Pav60 (0.75/4.5)	2302	5.1	1803	21	164.6	840

Table 1 – Observers contributing to 2018 September data of the IMO Video Meteor Network. Eff.CA designates the effective collection area; the overall number of nights is the number of nights with at least one camera operating, the overall observing time and number of meteors are sums over all cameras.

Table 1 – Observers contributing to 2018 September data of the IMO Video Meteor Network – continued from previous page.

Code	Name	Location	Camera	FOV [°²]	Stellar LM [mag]	Eff.CA [km²]	Nights	Time [h]	Meteors
MARRU	Marques	Lisbon/PT	Ran1 (1.4/4.5)	4395	4.0	1330	26	211.8	565
MASMI	Maslov	Novosibirsk/RU	Nowatec (0.8/3.8)	5559	3.6	827	4	32.8	198
MOLSI	Molau	Seysdorf/DE	Avis2 (1.4/50)*	1204	6.9	5982	25	169.4	1850
			Dimcam1 (0.8/8)	1553	6.8	10447	15	86.5	958
			Escimo2 (0.85/25)	154	8.1	3828	22	168.5	437
			Mincam1 (0.8/8)	1476	5.0	1286	10	49.9	237
		Ketzür/DE	Remo1 (0.8/8)	1467	6.5	5459	29	176.5	1359
			Remo2 (0.8/8)	1479	6.4	5037	30	183.7	991
			Remo3 (0.8/8)	1422	6.4	4207	29	203.9	1161
			Remo4 (0.8/8)	1478	6.5	5355	29	205.0	1574
MORJO	Morvai	Fülöpszállás/HU	Huful (1.4/5)	3666	3.8	805	26	217.2	306
MOSFA	Moschini	Rovereto/IT	Rover (1.4/4.5)	3868	4.2	1240	27	204.3	419
NAGHE	Nagy	Budapest/HU	Hukon (0.8/3.8)	5475	4.0	1583	27	209.9	740
		Piszkéstető/HU	Hupis (0.8/3.8)	5622	4.0	1539	5	24.0	58
		Zamardi/HU	Huzam (0.8/6)	2359	4.7	1340	17	152.9	425
OCHPA	Ochner	Albiano/IT	Albiano (1.2/4.5)	3013	4.3	886	25	161.6	307
OTTMI	Otte	Pearl City/US	Orie1 (1.4/5.7)	2317	3.8	373	21	36.0	164
PERZS	Perkó	Becsehely/HU	Hubec (0.8/3.8)*	5557	2.9	470	14	121.8	200
ROTEC	Rothenberg	Berlin/DE	Armefa (0.8/6)	2359	4.5	907	27	168.4	395
SARAN	Saraiva	Carnaxide/PT	Ro1 (0.75/6)	2354	4.0	536	23	172.0	243
			Ro2 (0.75/6)	2365	4.1	635	25	237.7	408
			Ro3 (0.8/12)	720	5.7	1126	27	251.5	476
			Ro4 (1.0/8)	1568	4.2	546	26	229.8	190
			Sofia (0.8/12)	726	4.8	516	25	223.1	328
SCALE	Scarpa	Alberoni/IT	Leo (1.2/4.5)*	4170	4.5	2044	26	177.0	260
SCHHA	Schremmer	Niederkrüchten/DE	Doraemon (0.8/3.8)	5522	4.7	3184	25	163.4	550
SLAST	Slavec	Ljubljana/SI	Kayak1 (1.8/28)	1074	5.7	2642	23	150.7	242
			Kayak2 (0.8/12)	742	5.7	1052	24	166.4	243
STOEN	Stomeo	Scorze/IT	Min38 (0.8/3.8)	5587	4.5	2362	28	202.5	1250
			Noa38 (0.8/3.8)	5612	4.2	1889	28	217.5	1011
			Sco38 (0.8/3.8)	5583	4.8	3304	27	199.0	1269
STRJO	Strunk	Herford/DE	Mincam2 (0.8/6)	2355	5.6	3423	26	162.1	961
			Mincam3 (0.8/6)	2302	4.5	1150	26	147.1	321
			Mincam4 (0.8/6)	2274	4.7	1001	26	147.5	335
			Mincam5 (0.8/6)	1481	6.0	3200	25	162.8	573
			Mincam6 (0.8/6)	2396	5.3	2748	27	159.5	528
TEPIS	Tepliczky	Agostyán/HU	Huago (0.75/4.5)	2428	4.6	1247	23	169.0	561
			Humob (0.8/6)	2388	4.6	1225	26	207.7	619
WEGWA	Wegrzyk	Nieznaszyn/PL	Pav78 (0.8/6)	2376	4.4	1264	25	136.0	409
YRJIL	Yrjölä	Kuusankoski/FI	Finexcam (0.8/6)	2315	5.5	2769	25	150.0	519
ZAKJU	Zakrajšek	Petkovec/SI	Petka (0.8/8)	1431	5.6	1956	28	208.6	1333
			Tacka (0.8/12)	715	5.3	784	28	193.9	467
						Overall	30	14 421.8	54 899

* active field of view smaller than video frame

The International Meteor Organization

www.imo.net

Follow us on Facebook InternationalMeteorOrganization

Follow us on Twitter @IMOMeteors

Council

President: Cis Verbeeck,
Bogaertsheide 5, 2560 Kessel, Belgium.
e-mail: cis.verbeeck@scarlet.be

Vice-President: Juraj Tóth,
Fac. Math., Phys. & Inf., Comenius Univ.,
Mlynska dolina, 84248 Bratislava, Slovakia.
e-mail: toth@fmph.uniba.sk

Secretary-General: Robert Lunsford,
14884 Quail Valley Way, El Cajon,
CA 92021-2227, USA. tel. +1 619 755 7791
e-mail: lunro.imo.usa@cox.net

Treasurer: Marc Gyssens, Heerbaan 74,
B-2530 Boechout, Belgium.
e-mail: marc.gyssens@uhasselt.be
BIC: GEBABEBB
IBAN: BE30 0014 7327 5911
Bank transfer costs are always at your expense.

Other Council members:

Megan Argo, Jodrell Bank Centre for Astrophysics,
Alan Turing building, University of Manchester,
Oxford Road, Manchester, M13 9PL, UK.
e-mail: megan.argo@gmail.com

Javor Kac (see details under WGN)

Detlef Koschny, Zeestraat 46,
NL-2211 XH Noordwijkerhout, Netherlands.
e-mail: detlef.koschny@esa.int

Masahiro Koseki, 4-3-5 Annaka, Annaka-shi,
Gunma-ken 379-0116, Japan.
e-mail: geh04301@nifty.ne.jp

Sirko Molau, Abenstalstraße 13b, D-84072 Seysdorf,
Germany. e-mail: sirko@molau.de

Jean-Louis Rault, Société Astronomique de France,
16, rue de la Vallée, 91360 Epinay sur Orge,
France. e-mail: f6agr@orange.fr

Jürgen Rendtel, Eschenweg 16, D-14476 Marquardt,
Germany. e-mail: jrendtel@aip.de

Galina Ryabova, Res. Inst. of Appl. Math. & Mech.,
Tomsk State University, Lenin pr. 36, build. 27,
634050 Tomsk, Russian Federation.
e-mail: ryabova@niipmm.tsu.ru

Damir Šegon, J. Rakovca 3, 52100 Pula, Croatia.
e-mail: damir.segon@pu.t-com.hr

Commission Directors

Visual Commission: Rainer Arlt (rarlt@aip.de)
Generic e-mail address: visual@imo.net
Electronic visual report form:
http://www.imo.net/visual/report/electronic

Video Commission: Sirko Molau (video@imo.net)

Photographic Commission: Bill Ward
(William.Ward@glasgow.ac.uk)
Generic e-mail address: photo@imo.net

Radio Commission: Jean-Louis Rault (radio@imo.net)

Fireballs: Online fireball reports:
http://fireballs.imo.net

Outreach Officer

Jure Atanackov, e-mail: jureatanackov@gmail.com

Webmaster

Karl Antier, e-mail: webmaster@imo.net

WGN

Editor-in-chief: Javor Kac
Na Ajdov hrib 24, SI-2310 Slovenska Bistrica,
Slovenia. e-mail: wgn@imo.net;
include METEOR in the e-mail subject line

Editorial board: Ž. Andreić, M. Argo, D.J. Asher,
F. Bettonvil, J. Correira, M. Gyssens,
C. Hergenrother, T. Heywood, J.-L. Rault,
J. Rendtel, C. Verbeeck, S. de Vet, D. Vida.

IMO Sales

Available from the Treasurer or the Electronic Shop on the IMO Website	€	$
IMO membership, including subscription to WGN Vol. 47 (2019)		
Surface mail	26	32
Air Mail (outside Europe only)	49	60
Electronic subscription only	21	25
Proceedings of the International Meteor Conference on paper		
1990, 1991, 1993, 1995, 1996, 1999, 2000, 2002, 2003, per year	9	12
2007, 2010, 2011, per year	15	20
2012, 2013, 2014, 2015 per year	25	34
Proceedings of the Meteor Orbit Determination Workshop 2006	15	20
Radio Meteor School Proceedings 2005	15	20
Handbook for Meteor Observers	15	20
Meteor Shower Workbook	12	16
Electronic media		
Meteor Beliefs Project ZIP archive	6	8

The 2019 April 16 fireball over Germany

Fireball from 2019 April 16, $21^{h}51^{m}$ UT, recorded by AllSky6 camera AMS16 from Ketzür, Germany. Image courtesy: Sirko Molau.

The fireball has also been recorded by AllSky6 camera AMS22 from Lindenberg, Germany, as well as by FRIPON cameras DEBB01, DENI01, NLEN01 and Denekamp. From these stations, a trajectory could be calculated. The visible trajectory started at 90 km and ended at slightly over 40 km over northern Germany with some fragmentation. The initial velocity of the meteoroid was about 30 km/s and the terminal velocity was near 25 km/s. The extension of the trail intersects the Earth surface close to Hamburg.

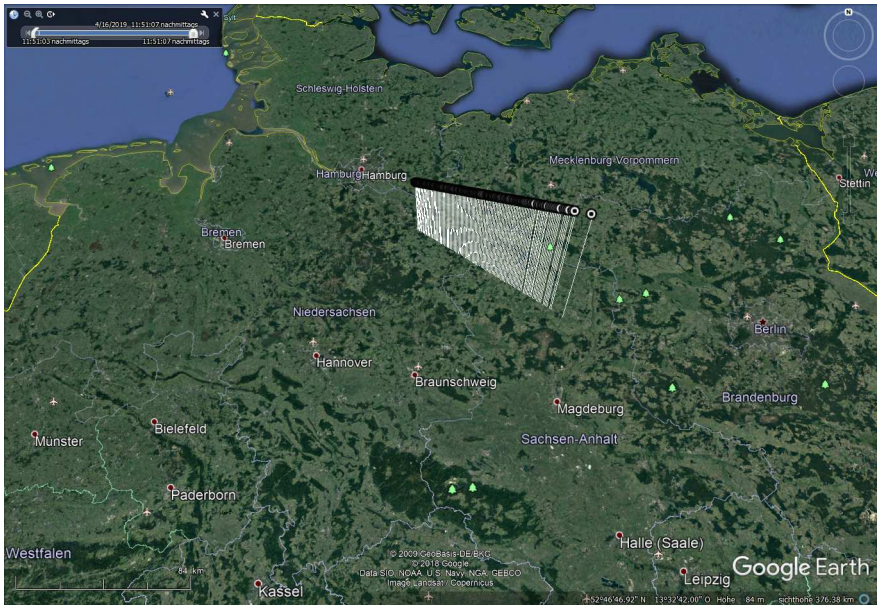

There are 74 fireball reports for this event:
`https://fireballs.imo.net/members/imo_view/event/2019/1774`